Supplementary methods

Reagents. Antibodies were obtained from the following companies. Abcam: anti-NANOG (ab21624), anti-H3K9me3 (ab8898), anti-emerin (ab14208), anti-Nup358 (ab64276), anti-Ki67 (ab16667), anti-Islet 1 (ab20670), anti-Ku70 (ab2172), anti-TPR (ab84516), anti-MSI1 (ab52865); Santa Cruz Biotechnology: anti-OCT-3/4 (sc-5279), anti-SOX2 (sc-17320), anti-HDAC1 (sc-7872), anti-HSP60 (sc-13966), anti-14-3-3 (sc-926), anti-Lamin A/C (sc-6215), anti-Lamin B1 (sc-6217), anti-TOM20 (sc-11415), anti-TAF II p135 (sc-136093); anti-Map2 (sc-32791); Cell Signaling: anti-HP1α (2616), p-4E-BP1 (2855), anti-cleaved caspase-3 (9661), anti-cleaved PARP (9541), anti-phospho-(Ser/Thr) kinase substrate antibody sampler kit (9920), anti-ERK5 (3372), anti-phospho-ERK5 (Thr218/Tyr220)(3371); Millipore: anti-TRA-1-60 (MAB4360), anti-tyrosine hydroxylase (TH) (AB152), anti-ChAT(AB144P), anti-nestin (MAB5326), anti-H3K27me3 (07-449), anti-acetyl-Histone H3 (AC-H3) (06-599); Sigma: anti-β-Tubulin III/TujI (T2200), anti-Flag (M2), anti-tubulin (T5168); anti-LRRK2 (L9918); BD Transduction Laboratories: anti-LAP2β (611000); Covance: anti-PAX6 (PRB-278P), Pol-II (8WG16/MMS-126R); Invitrogen: anti-Lamin B2 (33-2100); Active motif: anti-H3K4me3(39159). Anti-Ser935-LRRK2 rabbit monoclonal antibody was obtained from Division of Signal Transduction Therapy, University of Dundee. LRRK2-In-1 was purchased from EMD Chemicals. H-1152 was purchased from Santa Cruz Biotechnology. All other chemicals were purchased from Sigma. pMXs-OCT4, pMXs-SOX2, and pMXs-KLF4 plasmids were purchased from Addgene (17217, 17218, and 17219, respectively). Flag-LRRK2(wt) and Flag-LRRK2(G2019S) were kindly provided by Dr. Y. Imai [1]. Venus cDNA was kindly provided by Dr. A. Miyawaki [2].

Cells. Human Parkinson's disease fibroblasts FFF-028 (homozygous for *LRRK2* G2019S; male; 63 years old) and FFF-022 (heterozygous for *LRRK2* G2019S; male; 42 years old) were obtained from Telethon Genetic Biobank Network. Normal fibroblasts AG04444 (male; 63 years old) were purchased from Coriell Cell Repository. All fibroblast lines were cultured in DMEM (Invitrogen) containing 15% fetal bovine serum (FBS, HyClone), 0.1 mM non-essential amino acids (Invitrogen), 2 mM Glutamax (Invitrogen). H1 and H9 hESC lines were purchased from WiCell Research, and maintained in hESC medium [3].

iPSC generation and differentiation. Human iPSCs were generated as previously described [3], with minor modifications. In brief, human fibroblasts were infected with a mix of retroviruses encoding OCT4, SOX2, KLF4, and GFP. Five days after infection, fibroblasts were individualized and seeded onto fresh irradiated mouse embryonic fibroblasts (MEFs). The medium was then switched to hESC medium. After 28 days, colonies were picked onto MEF feeder cells for two passages and then transferred onto Matrigel (BD Biosiences)/mTeSR (Stemcell techonology) conditions. For embryoid body (EB) formation, iPSC colonies growing on MEFs were detached with dispase (Invitrogen), resuspended in IMDM medium (Invitrogen) supplemented with 0.1 mM non-essential amino acids, 2 mM GlutaMAX, 15% FBS (Gemini Atlanta Biologicals), and 55 μM β-mercaptoethanol (Invitrogen) and transferred to low attachment 6-well plates (Costar) for 6 days. EBs were then plated on gelatin-coated plates and maintained for another 14 days.

Derivation of NSCs from hiPSCs or hESCs. Neural induction was based on a previous report [4] with minor modifications. To start the induction, hESCs or hiPSCs were passaged onto MEF feeder cells at about 20% confluence with dispase. Culture medium was then switched to Neural Induction Medium 1 (NIM-1: 50% Advanced DMEM/F12 (invitrogen), 50% Neurobasal (invitrogen), 1x N2 (invitrogen), 1x B27 (invitrogen), 2 mM GlutaMAX (Invitrogen) and 10 ng/mL hLIF (Millipore), 4 μM CHIR99021 (Cellagentech, premade in 10 mM DMSO solution), 3 μM SB431542 (Cellagentech, premade in 10 mM DMSO solution), 2 μM Dorsomorphin (Sigma), and 0.1 μM Compound E (EMD Chemicals Inc.). Cells were treated with NIM-1 for 2 days, and then switched to Neural Induction Medium 2 (NIM-2: 50% Advanced DMEM/F12, 50% Neurobasal, 1x N2, 1x B27, 2 mM GlutaMAX, 10 ng/mL hLIF, 4 μM CHIR99021, 3 μM SB431542 and 0.1 μM Compound E) for another 5 days. The cultures were then split onto Matrigel-coated plates with Accumax (Innovative Cell Technologies) and cultured in Neural Stem cell Maintenance Medium (NSMM)

containing 50% Advanced DMEM/F12, 50% Neurobasal, 1x N2, 1x B27, 2 mM GlutaMAX, 10 ng/mL hLIF, 3 μM CHIR99021, and 2 μM SB431542.

NSC culture. NSCs were maintained on Matrigel in NSMM. NSCs were passaged once 80 to 100% confluent using Accumax and seeded at a 4 x 10^5 cells/ 35 mm well (Cytoone). Medium was changed every day. For the initial 6 passages, NSCs were treated with 10 μM Y-27632 (Biomol Inc.) during splitting. From passage 7 to 14, cells were maintained in NSMM. After passage 14, NSCs were cultured in NSMM supplemented with 5 μg/ml BSA (MP Biomedicals). We noticed that the quality of some NSC differentiation/culture medium components including N2, B27, and CHIR99021 vary from batch to batch and using certain batches of these products leads to delay or failure in identifying 'aged' phenotypes. In this regard, quality control of different batches of these products is required before experiments.

Clonal expansion assay. To determine the clonal expansion efficiency of NSCs, 2,000 cells were seeded onto a Matrigel-coated 35 mm well. Cells were cultured in NSMM for 1 week, and the relative colony number was then determined by microscopic measurement.

Single-cell based neuronal differentiation assay. For spontaneous neuronal differentiation, 2,000 NSCs were plated onto a Matrigel-coated 35 mm well, and maintained in NSMM for 3-5 days. The cultures were then switched into differentiation medium containing DMEM/F12, 1x N2, 1x B27, 400 μM dbcAMP (Sigma), 200 μM Ascorbic acid (Sigma), 10 ng/ml BDNF (Peprotech), and 10 ng/ml GDNF (Peprotech). Two days after being switched to differentiation medium, laminin (Sigma) was added to the cultures to facilitate differentiation. Cells were maintained in differentiation medium for 14 days in total, and then immunostained with neuronal markers MAP2 or Tuj1. For directed motor neuron differentiation, 2,000 NSCs were cultured in a Matrigel-coated 35 mm well in NSMM for 5 days, followed by commencement of a motor neuron differentiation protocol as previously described [4].

Differentiation towards dopaminergic neurons. Directed differentiation of hiPSCs into dopaminergic neurons was performed as previously described [5]. To differentiate NSCs into dopaminergic neurons, NSCs were dissociated to form suspended neurospheres using Lipidure-Coat U-bottom 96-Plates (NOF AMERICA CORPORATION). Neurospheres were cultured for 20 days in DA1 medium containing 50% Advanced DMEM/F12, 50% Neurobasal, 1x N2, 1x B27, 200 μM Ascorbic Acid, 2 μM Purmorphamine (Calbiochem), and 100 ng/ml FGF8 (Humanzyme). Neurospheres were then dissociated and seeded on coverslips, and cultured in DA2 Medium (Neurobasal, 1x N2, 1x B27, 200 μM Ascorbic Acid, 10 ng/ml BDNF, 10 ng/ml GDNF, 1 ng/ml TGF-b3 (Peprotech), 400 μM dbcAMP, 2 μM Purmorphamine, and 100 ng/ml FGF8) for 21 days. The generated neurons were maintained in DA3 medium (Neurobasal, 1x N2, 1x B27, 200 μM Ascorbic Acid, 10 ng/ml BDNF, 10 ng/ml GDNF, 1 ng/ml TGF-b3 and 400 μM dbcAMP) for another 1-2 months.

MudPIT proteomic analysis. The immunoprecipitation for MudPIT was carried out as previously described [3, 6]. Briefly, HEK293T cells were transfected with Flag-LRRK2(G2019S) or empty vector. 48 h later, the cells were lysed in ice-cold lysis buffer (200 mM NaCl, 0.5% Triton X-100, 50 mM Tris, pH 7.5, 1 mM EGTA, 1 mM EDTA, 10% glycerol, PhosSTOP, and complete protease inhibitor cocktail (Roche Diagnostics)). Flag-LRRK2(G2019S) and its associated proteins were immunoadsorbed to anti-Flag agarose. After extensive washing, the immunoprecipitates were eluted into 8 M urea (pH 8.5), and subjected to MudPIT proteomic analysis [3, 6, 7]. The hits identified uniquely in the Flag-LRRK2(G2019S)-expressed sample but not in the mock-transfected sample represent proteins that are specifically present in LRRK2(G2019S)-containing protein complexes.

Protein and mRNA analysis. For immunoblotting, cells were lysed in SDS sample buffer or ice-cold lysis buffer (200 mM NaCl, 0.5% Triton X-100, 50 mM Tris (pH 7.5), 1 mM EGTA, 1 mM EDTA, 10% glycerol, PhosSTOP, and complete protease inhibitor cocktail). Protein quantification

was performed with BCA kit (Thermo Fisher Scientific). Protein lysates from 40,000 cells or of 20 μg were subjected to Novex 4-12% Bis-Tris Gel (invitrogen) and immunoblotting analysis according to the previously described method [6]. TRIzol (Invitrogen) was used to extract total RNA. cDNA was synthesized using High Capability RNA-to-cDNA Mater Mix (Invitrogen). Quantitative RT-PCR followed using SYBR Green PCR Master Mix (Applied Biosystems). Primer sequences are given in **Supplementary Table 4.**

Immunofluorescence microscopy. Cells were fixed for 20 min in 4% formaldehyde in PBS at room temperature (RT). Subsequently, samples were treated with 0.4% Triton X-100 in PBS at RT for 10 min. Cells were blocked with 10% FBS in PBS for 1 h, and then incubated at 4°C overnight with primary antibody. Cells were washed in PBS and incubated at RT for 1 h with the corresponding secondary antibody. DNA was stained with Hoechst 33342 (Invitrogen). RNA was stained with SYTO® RNASelect™ Green Fluorescent Cell Stain (Invitrogen). Quantitative microscopy was performed using around 100 randomly chosen cells for each sample. Nuclear envelope circularity and nuclear area were calculated using Image J (NIH).

3D fluorescence *in situ* hybridization (3D-FISH). Cy3-labeled Centromere PNA probe and FAM-labeled Telomere PNA probe were purchased from Panagene. Cells were fixed in 4% formaldehyde for 10 min at RT, permeabilized with Triton X-100 and repeat freezing in liquid nitrogen. Deproteinization was performed by treatment with 0.1 M HCl. Hybridization was carried out at RT for 1 h. Post hybridization washes were in 0.1X SSC at 60°C. Samples were counterstained with DAPI, mounted and examined using a Zeiss LSM 780 Laser Scanning Confocal Microscope (Zeiss).

Teratoma analysis. To test for pluripotency *in vivo*, teratoma formation was assessed following injection of iPSC lines into NOD-SCID IL2Rgamma^{null} mice (Jackson Laboratories). In short, 10^6 iPSCs were injected into the testis of anaesthetized mice and teratoma formation was monitored. Animals were sacrificed ~6-12 weeks after injection. Immunostaining and hematoxylin-eosin (H&E) staining were used to analyse harvested teratomas. All murine experiments were conducted with approval of The Salk Institute Institutional Animal Care and Use Committee (IACUC).

Bisulfite sequencing of the *OCT4* promoter. Bisulfite conversion of DNA was carried out using the Zymo EZ DNA Methylation-direct Kit (Zymo Research) following the manufacturer's suggestions. In brief, following extraction of genomic DNA, a fragment of the *OCT4* promoter was amplified with 2x Zymo Taq Premix, as directed by the manufacturer, and previously published primers [8]. PCR products from at least 8 clones were cloned into the pCR2.1-TOPO vector (Invitrogen) and sequenced with M13 universal primer.

ChIP-seq. Dynabeads M-280 Sheep anti-Mouse IgG (Invitrogen) or Dynabeads M-280 Sheep anti-Rabbit IgG (Invitrogen) were washed 3 times with 5 mg/ml BSA (Sigma-Aldrich) in PBS. 3 μg of anti-H3K4me3 antibody (Millipore) were added to the beads in BSA/PBS and incubated for 2 h at 4°C. The antibody-bound beads were washed 3 times with BSA/PBS and incubated with 20 ⌠g of chromatin and a master mix of 1% Triton X-100, 0.1% DOC, 1x Protease inhibitors (Roche), and 1x TE, at 4°C overnight on a rotator. Samples were washed 5 times with RIPA Buffer (50 mM Hepes-KOH, pH8.0, 1 mM EDTA, 1% NP-40, 0.7% DOC, 0.5 M LiCl, 1x Protease inhibitors) and once with 1x TE. Samples were eluted with Elution Buffer (10 mM Tris-HCl [pH8.0], 1 mM EDTA, 1% SDS), incubated at 65°C for 20 min in a Thermomixer (Eppendorf), and reverse crosslinked at 65°C overnight with input chromatin. Eluted samples were treated with 0.2 mg/ml RNase A (Sigma-Aldrich) and 0.4 mg/ml Proteinase K (New England Biolabs (NEB)) for 1 h each. DNA was precipitated by phenol extraction using Phenol:Chlroform:Isoamyl Alcohol (Sigma-Aldrich) and Phase Lock Gel tubes (5 Prime). 200 mM NaCl and 100% ethanol were added to the samples, which were then incubated at -80°C for 30 min and spun at 14,000 rpm for 15 min at 4°C. Pellets were washed with 70% ethanol, air-dried to resuspend with 1 μg of RNase A in 1x TE, and incubated for 3 min at 37°C. Samples were purified using QIAquick PCR Purification Kit (Qiagen) and stored at -20°C. Chromatin-immunoprecipitated DNA ends were modified with End-

it DNA End-repair Kit (Epicentre Technologies). Adapters were ligated to the ends of the DNA fragments using Quick Ligation Kit (NEB) and Adapter Oligo mix from the Illumina Oligo Kit (Illumina Inc). Ligation products were purified by 2% agarose gel electrophoresis. DNA fragments ranging from 200 bp to 400 bp were selected and extracted in EB buffer (Qiagen). Selected fragments were amplified with PCR Primers and Indexes from Illumina's Kit and Phusion Hot Start High-Fidelity DNA Polymerase (NEB). Fragments were then purified with QIAquick PCR Purification Kit (Qiagen). DNA fragments from 200 bp to 400 bp were selected again by 2% agarose gel electrophoresis. Selected fragments were eluted in EB buffer. The resulting DNA was quantified with Qubit by the manufacturer's protocol and was diluted to 10 nM for sequencing. Sequencing of the libraries was performed as previously described [9]. The 36-bp sequence reads were aligned to the reference sequence, which consisted of hg18 (NCBI Build 36, March 2006), *H.sapiens* genome using Bowtie software [10]. Up to two mismatches with the reference sequence were allowed. Unique monoclonal reads were selected and genome browser files were constructed using SAMtools [11] , Picard (http://picard.sourceforge.net/index.shtml) and BEDtools (Quinlan). Perl was used to extract the number of reads per ared +/- 2.5kb up- and downstream of TSS of RefSeq gene. R/Bioconductor was used for quantile normalization, correlation and scatter plot analysis of the read counts. Gene ontology analysis was carried out using DAVID Bioinformatics Resource [12]. For genome wide display of read densities, the UCSC genome browser was used. CHIP-seq data have been deposited in NCBI-GEO with the accession number GSE34061. The following link has been created to allow review of record GSE34061: http://www.ncbi.nlm.nih.gov/geo/query/acc.cgi?token=jjwdjosyqiwuihg&acc=GSE34061

DNA microarray and bioinformatics analysis. Fibroblasts, ESC and iPSC samples were prepared in biological duplicates. NSC samples were prepared in biological triplicates. Total RNA of all samples was extracted using Trizol Reagent (Invitrogen) and purified by RNeasy Mini Kit (QIAGEN). Affymetrix GeneChip microarray processing was performed by the Functional Genomics Core Facility at the Salk Institute for Biological Studies according to the manufacturer's protocol (Affymetrix, Santa Clara, CA). Briefly, 100 ng of total RNA of each sample was processed using Affymetrix GeneChip 3' IVT Expression Kit following the manufacturer's protocol. For each sample, 12.5 μg fragmented and labeled aRNA were hybridized to the Affymetrix HG-U133A 2.0 chips. Expression signals were scanned on an Affymetrix GeneChip Scanner 3000 7G. The statistical analysis of the data was performed on the GenePattern platform from the Broad Institute (http://www.broadinstitute.org/cancer/software/genepattern/). Briefly, raw CEL files were imported into GenePattern software and normalized using RMA algorithm. The Hierarchical Clustering analysis was performed using the HierarchicalClustering module of the GenePattern software. The dendrograms and the heat map of the clustered gene expression data were visualized by the HierarchicalClusteringViewer module. Microarray data for *LRRK2* G2019S iPSCs (**Supplementary Fig. 3g**) have been deposited in NCBI-GEO with the accession number GSE33298; microarray data for LRRK2-In-1-treated esNSCs-H9-LK2(GS/+) (**Fig. 4g**) have been deposited in NCBI-GEO with the accession number GSE36321.
The following link has been created to allow review of record GSE33298:
http://www.ncbi.nlm.nih.gov/geo/query/acc.cgi?token=bjuxbgquoqkyqdm&acc=GSE33298
And the following link has been created to allow review of record GSE36321:
http://www.ncbi.nlm.nih.gov/geo/query/acc.cgi?token=vpkxxmayiskiite&acc=GSE36321

Flow cytometry analysis. For cell apoptosis assays, NSCs were switched to BSA-containing NSMM for at least two passages, and then treated with or without MG132 (Calbiochem). Cells were collected, washed twice with PBS, and incubated with PI/FITC-Annexin V (BD, Annexin V: FITC Apoptosis Detection Kit I) for 30 min at RT. The cells were then washed once with binding buffer, and analyzed using LSRII (BD Bioscience). For measurement of mitochondrial membrane potential, NSCs were treated with vehicle or 50 μM CCCP (Sigma Aldrich) for 30 min, and then individualized into single cells. After exposure to 2 μg/ml JC-1 dye (Invitrogen) for 30 min at 37°C, cells were analyzed by LSRII (BD Biosciences).

Transmission electron microscopy. Cells were grown on 20 mm aclar coverslips and fixed in 2.5% glutaraldehyde (GA) in a 0.1M buffer of sodium cacodylate (pH 7.4). Post-fixation,

coverslips were buffer washed and treated to a secondary fixation in 1% Osmium Tetroxide (OsO4) and 1% Potassium Ferrohexacyanate (K3Fe(CN)6) in 0.1M cacodylate buffer. Coverslips were then washed with high-resistivity water and en bloc stained with 2% uranyl acetate followed by a graded acetone dehydration series with propylene oxide as an intermediate solvent. Samples were then rapidly infiltrated in Spurr's resin using a Pelco BioWave microwave (Ted Pella), flat embedded, and cured at 70˚C overnight. Regions of interest were found via light microscopy, excised from the flat molds and remounted on blank resin stubs. 70 nm ultrathin sections were cut on a Leica UC7 ultramicrotome (Leica) using a Diatome Ultra 35 diamond knife (Diatome) and mounted on formvar/carbon coated 100 hex mesh copper grids. Sections were not counterstained and examined at an 120 kV accelerating voltage on a Zeiss Libra 120 PLUS EF-TEM (Zeiss) and recorded using a 2kx2k Sharp:Eye fiber-optically coupled YAG CCD (TRS).

Construction and preparation of HDAdVs. *LRRK2*-c-HDAdV for gene correction and *LRRK2*-G2019S-HDAdV for mutation knock-in were generated using a BAC clone containing the human *LRRK2* locus (RP11-115F18, BACPAC Resources), that was modified using BAC Recombineering [13]. In brief, to construct gene-correction vector (*LRRK2*-c-HDAdV), the *FRT*-PGK-EM7-neo-bpA-*FRT* fragment was recombined into a site 270 bp downstream of exon 41 of *LRRK2* in the BAC clone. A total of 22.6 kb of *LRRK2* homology, including the marker cassette, was subcloned into the HDAdV plasmid pCIHDAdGT8-4 (kindly provided by Dr. Kohnosuke Mitani). To construct the mutation knock-in vector (*LRRK2*-G2019S-HDAdV), exon 41 of *LRRK2* was PCR-amplified from RP11-115F18 BAC DNA with the following primers: 5'-GATTTGACCCTTTTTTAAAGCATAA-3' and 5'-GCCTCACAAGTGCCAACAATAC-3' and subcloned into the pCR2.1-TOPO vector. The G2019S (G6055A) mutation was introduced with the following primers: 5'-TGCAAAGATTGCTGACTACAGCATTGCTCAG-3' and 5'-GTAGTCAGCAATCTTTGCAATGATGGCAG-3' using the GeneTailor Site-Directed Mutagenesis System (Invitrogen). An *FRT*-PGK-EM7-neo-bpA-*FRT* fragment was subcloned into a site 270 bp downstream of exon 41 in the G2019S mutated plasmid, and the generated DNA fragment was recombined into RP11-115F18 BAC DNA. A total of 22.6 kb of *LRRK2* homology, including the G2019S mutation and marker cassette, was subcloned into the HDAdV plasmid pAMHDAdGT8-4. The Venus-expression vector (pHDAdVenus-geo-TK) was kindly provided by Dr. Kohnosuke Mitani. To construct the LRRK2 G2019S over-expression HDAdV (pHDAdV(Venus)-LK2(GS)-Flag), Flag-LRRK2(G2019S) [1] was subcloned into pCMV-Myc (Clonetech). The CMV promoter-driven Flag-LRRK2(G2019S) cassette was subcloned into pHDAdVenus-geo-TK. The generated *LRRK2*-c-HDAdV, *LRRK2*-G2019S-HDAdV, pHDAdVenus-geo-TK and pHDAdV(Venus)-LK2(GS)-Flag plasmids were linearized by *Pme*I (NEB) and then transfected into 116 cells (kindly provided by Dr. Philip Ng) in the presence of helper virus AdHPBGF35 (kindly provided by Dr. André M. Lieber) [14]. Crude virus extracts were serially amplified in 116 cells and then purified according to a previously described method [15, 16]. bgal-transducing units (btu) and Venus-transducing units (vtu) were determined in 293 cells to define infectious vector titers.

Isolation of the gene-corrected hiPSC and mutation knock-in hESC clones. For generation of gene-corrected iPSCs, 2 x 10^6 feeder-free cultured heterozygous *LRRK2* G2019S patient iPSCs were dissociated by TrypLE (Invitrogen), and resuspended in 1ml of MEF-conditioned medium containing 10 μM ROCK inhibitor Y-27632. Cells were infected with *LRRK2*-c-HDAdV at multiplicity of infection (MOI) of 3 btu/cell at 37°C for 1 h, and after brief centrifugation resuspended in 10 ml MEF-conditioned medium containing 10 μM Y-27632. Cells were plated onto 100 mm dishes precoated with 1 x 10^6 irradiated neomycin-resistant MEFs (Applied Stem Cell). Two days after infection, G418 (50 μg/ml; Invitrogen) was added to the medium to start positive selection. After 10-14 days, 2 μM Ganciclovir (GANC; Invitrogen) in addition to G418 was added to the medium to start negative selection. After an additional 5-7 days, G418/GANC double-resistant clones were transferred to 96-well plates and expanded for further characterization. For generation of *LRRK2* G2019S mutation knock-in hESCs, 1.25 x 10^6 feeder-free cultured H9 hESCs were dissociated by TrypLE, and resuspended in 1ml MEF-conditioned medium containing 10 μM Y-27632. Cells were infected with *LRRK2*-G2019S-HDAdV at MOI of 3 btu/cell at 37°C for 1 h, and after brief centrifugation resuspended in 10 ml MEF-conditioned

medium containing 10 μM Y-27632. Cells were plated onto 100 mm dishes precoated with 1 x 10^6 irradiated neomycin-resistant MEFs. Two days after infection, G418 (100 μg/ml) was added to the medium to start positive selection. After 10-14 days, GANC (2 μM) in addition to G418 was added to the medium to start negative selection. After an additional 5-7 days, G418/GANC double-resistant clones were transferred to 96-well plates and expanded for further characterization. Gene-targeting efficiency was determined by PCR of genomic DNA from drug-resistant clones with the following primers (P1, 5'-AAGGCCTCCTGGGACTCAGCAGAAAGCTC-3'; P2, 5'-CCCCAAAGGCCTACCCGCTTCCATTGCTCA-3'; P3, 5'-CTACCTGCCCATTCGACCACCAAGCGAAACATC-3'; P4, 5'-AGGTACGCCATCCCCAGCTACCCTGA-3'; also see **Fig. 3a and Supplementary Fig. 13a**) with LA Taq Hot Start Version (TAKARA). Long PCR cycling included a 1 min initial denaturation at 94°C, 14 cycles of 20 sec denaturation at 94°C and a 12 min annealing and extension at 68°C, 21 cycles of 20 sec denaturation at 94°C and a 12 min ±5 sec/cycle annealing and extension at 68°C plus a final extension at 68°C for 10 min. To determine the gene-correction and mutation knock-in efficiencies, genomic DNA was extracted from the gene-targeted clones. Exon 41 of *LRRK2* was PCR-amplified with the following primers: 5'-ACAAAAGAAAAGTCTCCAAAAATTGGGTCTTTGCCTGAG-3' and 5'-CCATCCTGAAGATAGAATTATGAGACAGACCTGATCACC-3' with LA Taq Hot Start Version. Amplicons were sequenced by ABI 3730 sequencer (Applied Biosystems).

Excision of the neomycin-resistance cassette in *LRRK2* gene-corrected hiPSC and *LRRK2* G2019S knock-in hESC clones. To efficiently remove the neomycin-resistance cassette, we generated a pCAG-Flpo-2A-*puro* vector, which expresses the genes for Flpo recombinase [17] and puromycin N-acetyltransferase (*puro*) driven by a CAG promoter. *LRRK2* gene-corrected hiPSCs and *LRRK2* G2019S knock-in hESCs cultured on Matrigel were transfected with pCAG-Flpo-2A-*puro* vector using FuGENE HD (Roche). Two days after transfection, puromycin (1 μg/ml; Invitrogen) was added to the medium to enrich Flpo recombinase expressing cells. Two days later, puromycin was withdrawn, and after 1 week, the cells were individualized and plated onto MEF feeder cells at a density of 300-3000 cells / 75 cm^2 in the presence of 10 μM Y-27632. After 2 weeks, the emerging colonies were picked and expanded. The removal of the neomycin-resistance cassette was verified by PCR using LA Taq Hot Start Version and DNA sequencing with the following primers: 5'-ACCTCCACTCAGCCATGATTATATACCGAGACC-3' and 5'-GATGTTTCGCTTGGTGGTCGAATGGGCAGGTAG-3'.

Transduction of NSCs with HDAdV(Venus) or HDAdV(Venus)-LK2(GS)-Flag expression vector. For immunofluorescence analysis, wild-type ipsNSCs at passage 10 were plated onto Matrigel-coated 12-well plates. The next day, cells were infected with control vector HDAdV(Venus) or HDAdV(Venus)-LK2(GS)-Flag at MOI 30 at 37°C for 1 h in 300 μl of NSMM, and then an additional 700 μl of NSMM was added. Cells were subsequently subcultured on coverslips precoated with Matrigel. Cellular and nuclear morphology were examined by immunofluorescence microscopy 10 days after infection. For immunoprecipitation, 1.5 x 10^6 hESC-derived NSCs were plated on Matrigel-coated 100 mm dishes. The next day, cells were infected with 1 x 10^8 vtu of HDAdV(Venus) or HDAdV(Venus)-LK2(GS)-Flag at 37°C for 1 h in 2 ml of NSMM, followed by addition of an extra 8 ml of NSMM. Three days after infection, cells were lysed for immunoprecipitation.

Human brain samples immunostaining and quantification. Post-mortem human brain sections (5μm) of the hippocampal dentate gyrus and the cortex regions were obtained from the Biobank of hospital clinic (IDIBAPS) in Barcelona. Samples were selected from 11 age-matched individuals: 3 controls, 3 PD patients bearing the LRRK2(G2019S) mutation and 5 idiopathic PD patients. Of note, 2 out of 3 control patients (#0288 and #0319) were diagnosed for Alzheimer's disease (I-II Braak staging). Samples were fixed in 4% paraformaldehyde and a heat induced antigen retrieval step (5min in citrate buffer, pH. 9.0, in pressure cooker) was performed prior to staining. Sections were incubated for 1 hour at room temperature (RT) with blocking buffer (TBS with 0.5% Triton and 3% donkey serum) and for 24 hours at 4°C with the primary antibodies

diluted in blocking solution. Then, slices were rinsed (3 x 5 min) in TBS and incubated for 2 hours with cross-adsorbed fluor-conjugated secondary antibodies in dark conditions. After several washes in TBS, slices were counter-stained with 0.5 µg/ml DAPI for 30 min and mounted with anti-fading medium. Pictures (10 per patient) were acquired with a Leica SP5 AOBS confocal microscope and analyzed for quantification of the number of aberrant nuclei in the hippocampal dentate gyrus region as a mean percentage of the total number of nuclei calculated as follow: (number of nuclei with a “pedal-like” shape / total number of nuclei) x 100.

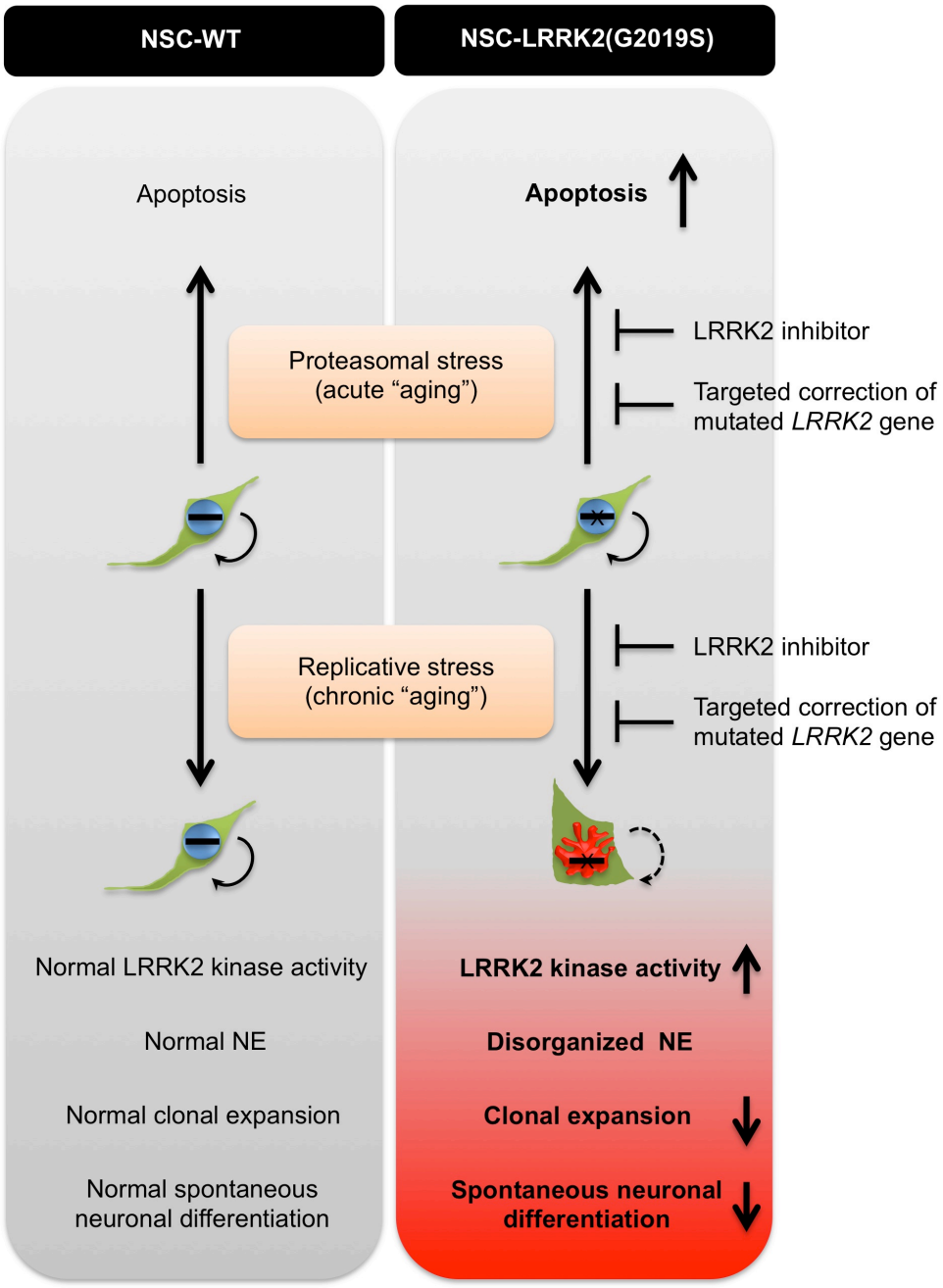

Supplementary Fig. 1. Schematic representation of *LRRK2*(G2019S)-associated NSC phenotypes. Upon challenges by proteasomal stress (which mimics acute aging) or replicative stress (which mimics chronic aging due to suboptimal culture conditions), *LRRK2*(G2019S) mutant NSCs show various abnormal cellular phenotypes including increased apoptosis, a disorganized nuclear envelope (NE), compromised clonal expansion and spontaneous neuronal differentiation capabilities. These aberrant phenotypes can be rescued by treatment with an LRRK2 inhibitor or targeted gene correction of the mutated *LRRK2* gene.

a

Nuclear lamina and matrix	Nuclear pores	Nuclear bodies	Chromatin-associated	Identified previously
Lamin B1	Nup153	PML	CBX3 (HP1Hs-gamma)	LRRK2
Lamin A/C	Nup62	Ki-67	RIF1	CDC37
LAP2α	Nup50	Nucleolin	ACINUS	HSP90
NUMA1	Nup358	ZRANB2	CENPF	14-3-3
Matrin-3	TPR	NPM1	DFFA	EF-1a
SAFB	RanBP1		53BP1	Tubulin
SAFB2			RBBP4	
			RBBP6	
			RBBP7	
			TAF-II	
			Reptin	
			p65	
			NAP2	

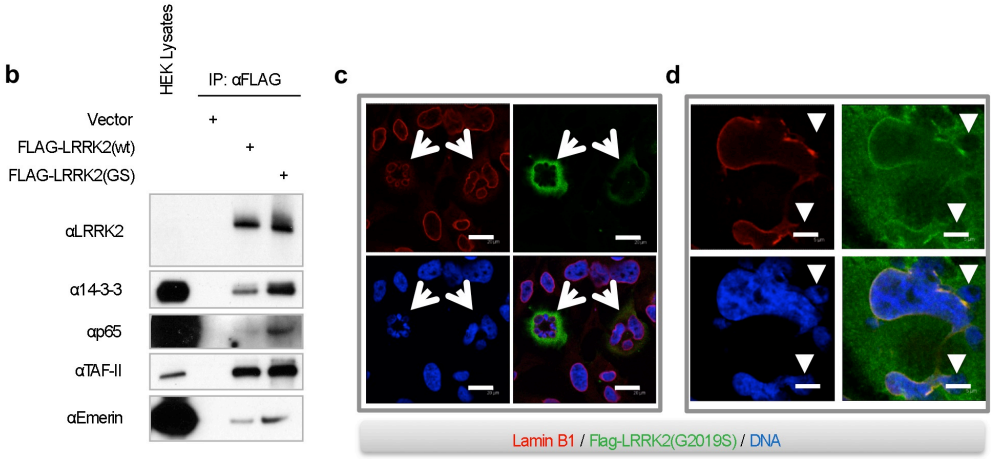

Supplementary Fig. 2. MudPIT proteomic analysis. a, LRRK2(G2019S)-associated nuclear components and chromatin-associated proteins identified by MudPIT proteomic analysis. Hits identified in this study include LRRK2, CDC37, HSP90, 14-3-3, EF-1α, and Tubulin, which have already been reported in other studies. See also **Supplementary Table 1. b**, Co-immunoprecipitation verification of a number of randomly selected hits identified above. Extracts from transfected HEK293 cells expressing empty vector, Flag-LRRK2(wt), or Flag-LRRK2(G2019S) were immunoprecipitated (IP) with an anti-Flag antibody, and then LRRK2-associated proteins were examined by immunoblotting with the indicated antibodies. **c-d,** HeLa-S4 cells were transiently transfected with Flag-LRRK2(G2019S). 48 h later, the cells were immunostained with the indicated antibodies. Arrows indicate Flag-LRRK2(G2019S)-expressing cells with disorganized nuclear architecture (**c**), and arrowheads denote the nuclear microdomains deficient for Lamin B1 (**d**). Scale bars, 20 μm (**c**), and 5 μm (**d**).

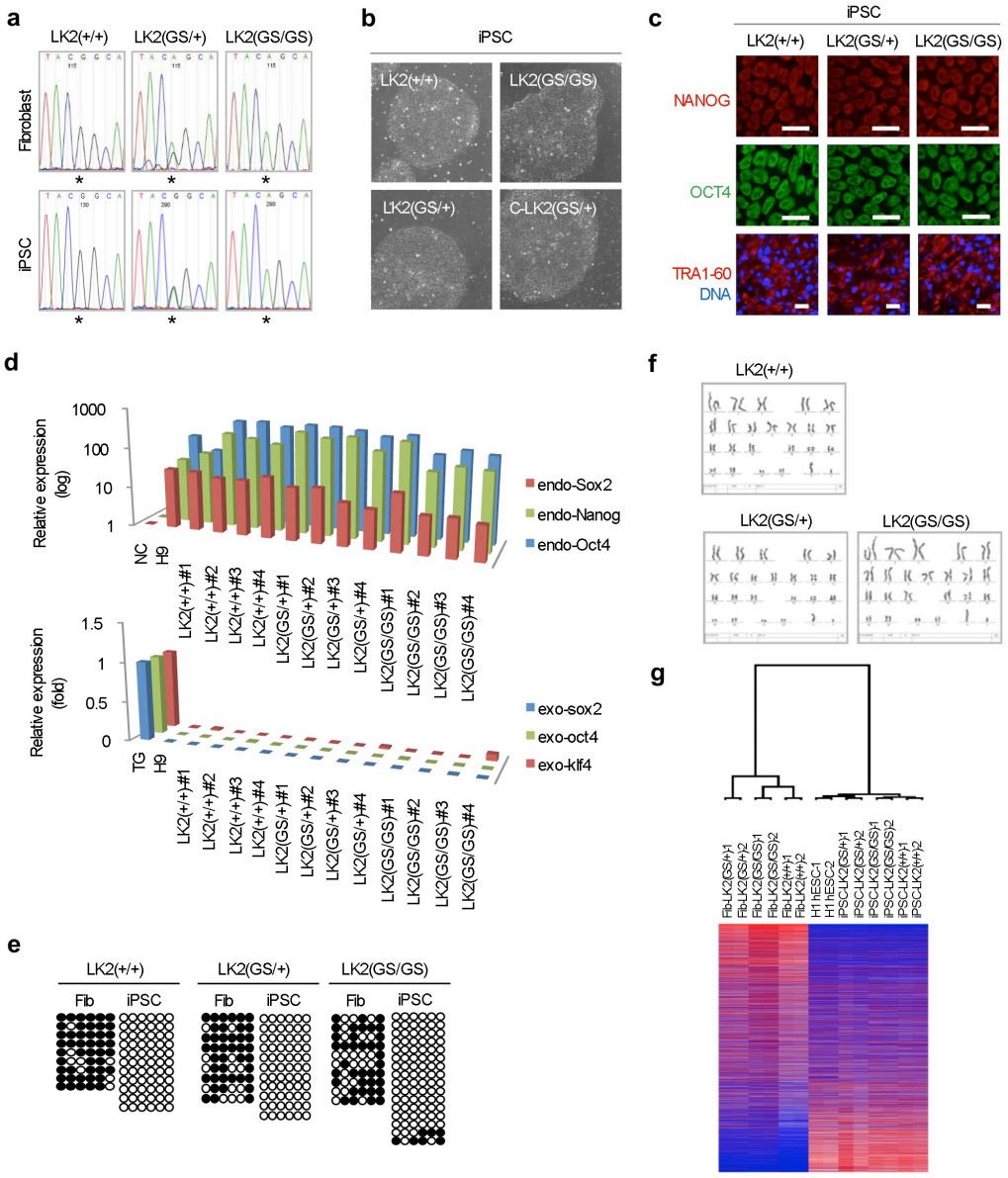

Supplementary Fig. 3. Characterization of iPSCs derived from control and patient fibroblasts bearing the *LRRK2* G2019S mutation. a, DNA sequencing analysis in wild-type and *LRRK2*-mutated fibroblast and iPSC lines revealed the presence of heterozygous and homozygous G2019S point mutations in *LRRK2*. **b,** Cell morphology of specific iPSC lines (passage 40) derived from fibroblasts of a healthy individual [LK2(+/+)], and two LRRK2-mutant individuals [heterozygous LK2(GS/+) and homozygous LK2(GS/GS)], as well as a gene-corrected iPSC line [C-LK2(GS/+)]. **c,** Immunofluorescence analysis of pluripotency markers in the indicated cell lines. DNA was counterstained with Hoechst. Scale bars, 20 μm. **d,** Quantitative PCR analysis of endogenous (endo) pluripotent genes and exogenous (exo) transgenes in the indicated iPSC lines. H9 hESCs were included as a positive control and BJ fibroblasts were included as a negative control (NC); BJ fibroblasts infected with retroviruses encoding OCT4, SOX2, and KLF4, were included as controls for transgene expression (TG). **e,** DNA methylation status of the *OCT4* promoter in the generated iPSCs and their parental fibroblasts. **f,** The generated iPSC lines exhibited normal karyotypes. **g,** Hierarchical clustering analysis of global gene expression profiles for the indicated iPSC lines and their parental fibroblast lines. H1 hESCs were included as a control.

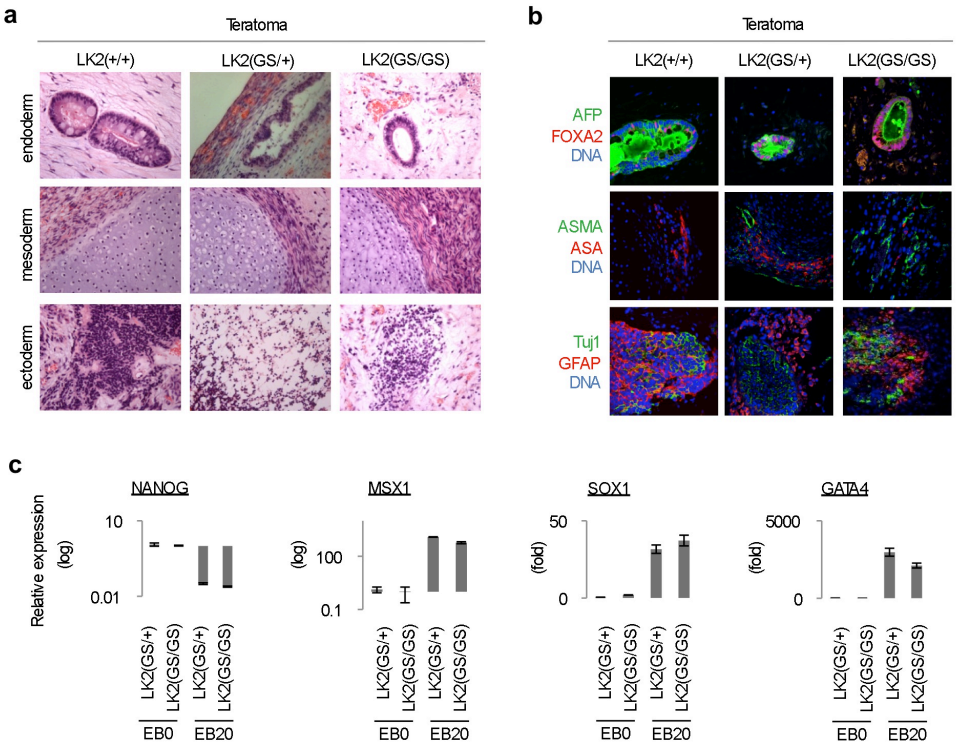

Supplementary Fig. 4. iPSCs demonstrate all hallmarks of pluripotency. a-b, H&E- (**a**) and immunofluorescence (**b**) staining in iPSC-derived teratomas comprising three germ layers. **c,** Quantitative PCR analysis of pluripotency marker Nanog, and differentiation markers MSX1, SOX1 and GATA4 in *LRRK2* mutant iPSCs cultured on matrigel (EB0) and subsequently differentiated as embryoid bodies towards the three germ layers of the embryo at day 20 (EB20). Data are shown as mean±s.d. n=3.

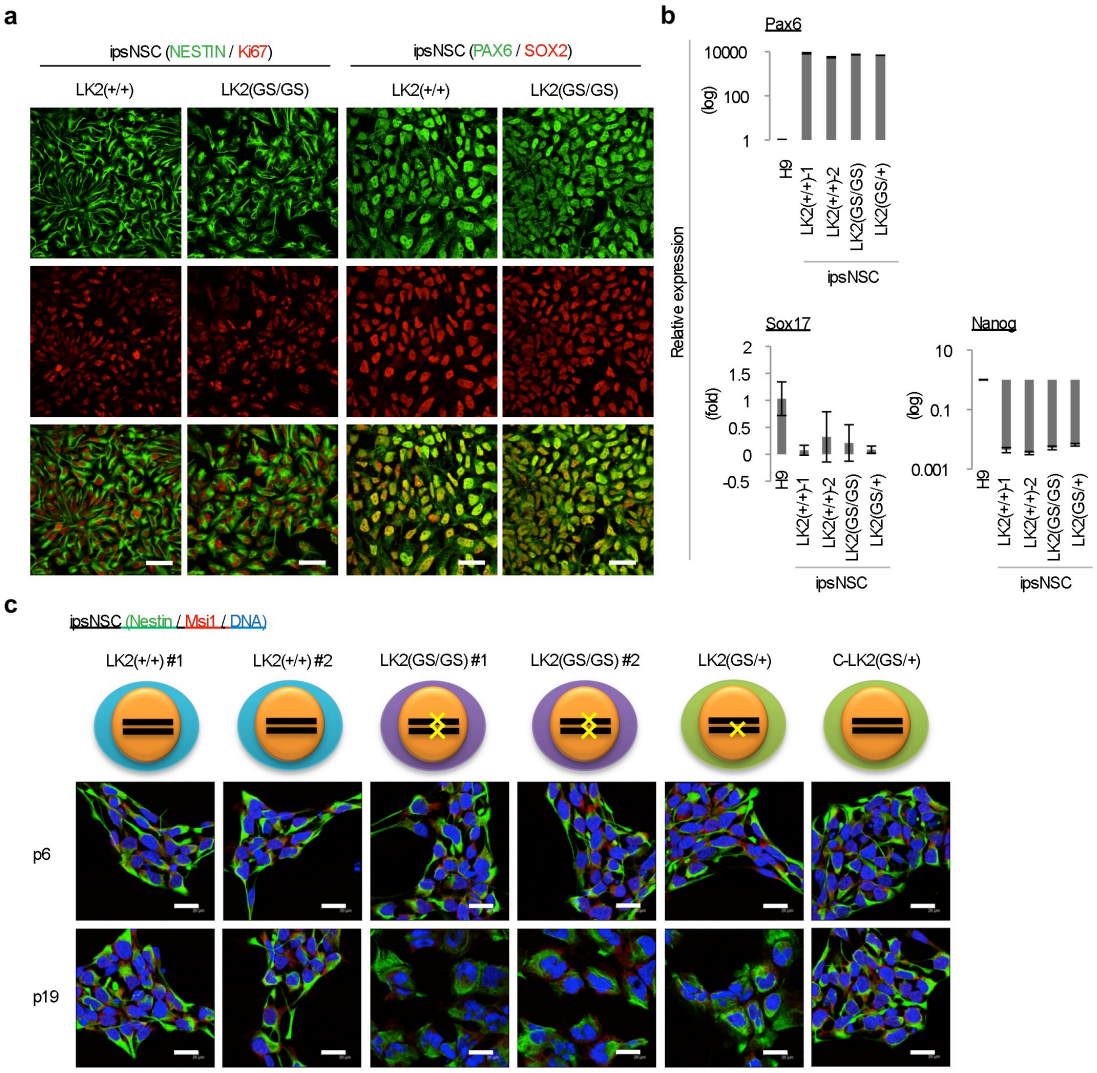

Supplementary Fig. 5. Characterization of ipsNSCs. a-b, Immunofluorescence (**a**) and quantitative PCR analysis (**b**) for the indicated neural progenitor and pluripotency markers in iPSC-derived NSCs (ipsNSCs) at passage 6. Scale bars, 40 μm. Data are shown as mean±s.d. n=3. **c,** Immunostaining of Nestin and Msi1 in the indicated ipsNSC lines at passage 6 (p6) and passage 19 (p19). DNA was counterstained with Hoechst. Scale bars, 20 μm.

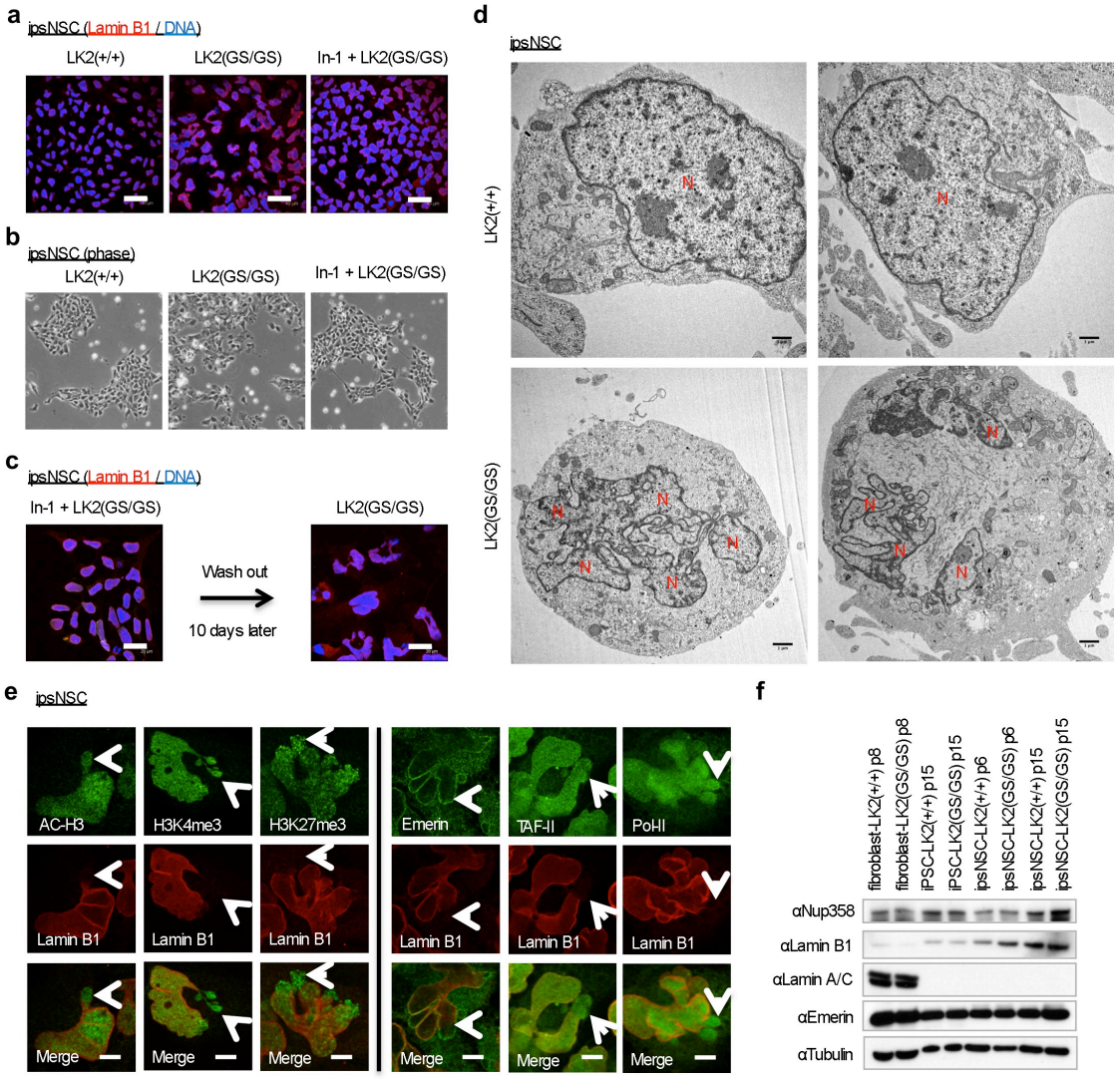

Supplementary Fig. 6. Cellular and nuclear morphology of *LRRK2* G2019S mutant ipsNSCs. **a-b,** Examination of Lamin B1 (**a**) and cellular morphology (**b**) in passage 15 ipsNSCs-LK2(GS/GS) treated with 3 μM LRRK2 inhibitor (In-1) for 4 (**a**) or 8 days (**b**). ipsNSCs-LK2(+/+) at passage 15 were used as controls. Scale bars, 40 μm. **c**, In-1 treated ipsNSCs-LK2(GS/GS) indicated in (**b**) were washed twice with medium and subsequently cultured in In-1 free medium for an additional 10 days. Staining of Lamin B1 revealed the reappearance of deformed nuclei. DNA was counterstained with Hoechst. Scale bars, 20 μm. **d**, Transmission electron microscopy analysis in passage 19 ipsNSCs-LK2(+/+) and ipsNSCs-LK2(GS/GS). Representative cells from each line are shown. ipsNSCs-LK2(GS/GS) show highly folded, deformed nuclei. N, nucleus. Scale bars, 1 μm. **e**, Immunofluorescence analysis indicates the expression of various nuclear components in Lamin B1-deficient nuclear microdomains in ipsNSCs-LK2(GS/GS) at passage 15. Arrows denote nuclear microdomains deficient for Lamin B1. Scale bars, 5 μm. **f,** Immunoblotting analysis of the indicated nuclear envelope proteins in fibroblasts, iPSCs, and ipsNSCs. Tubulin was used as a loading control.

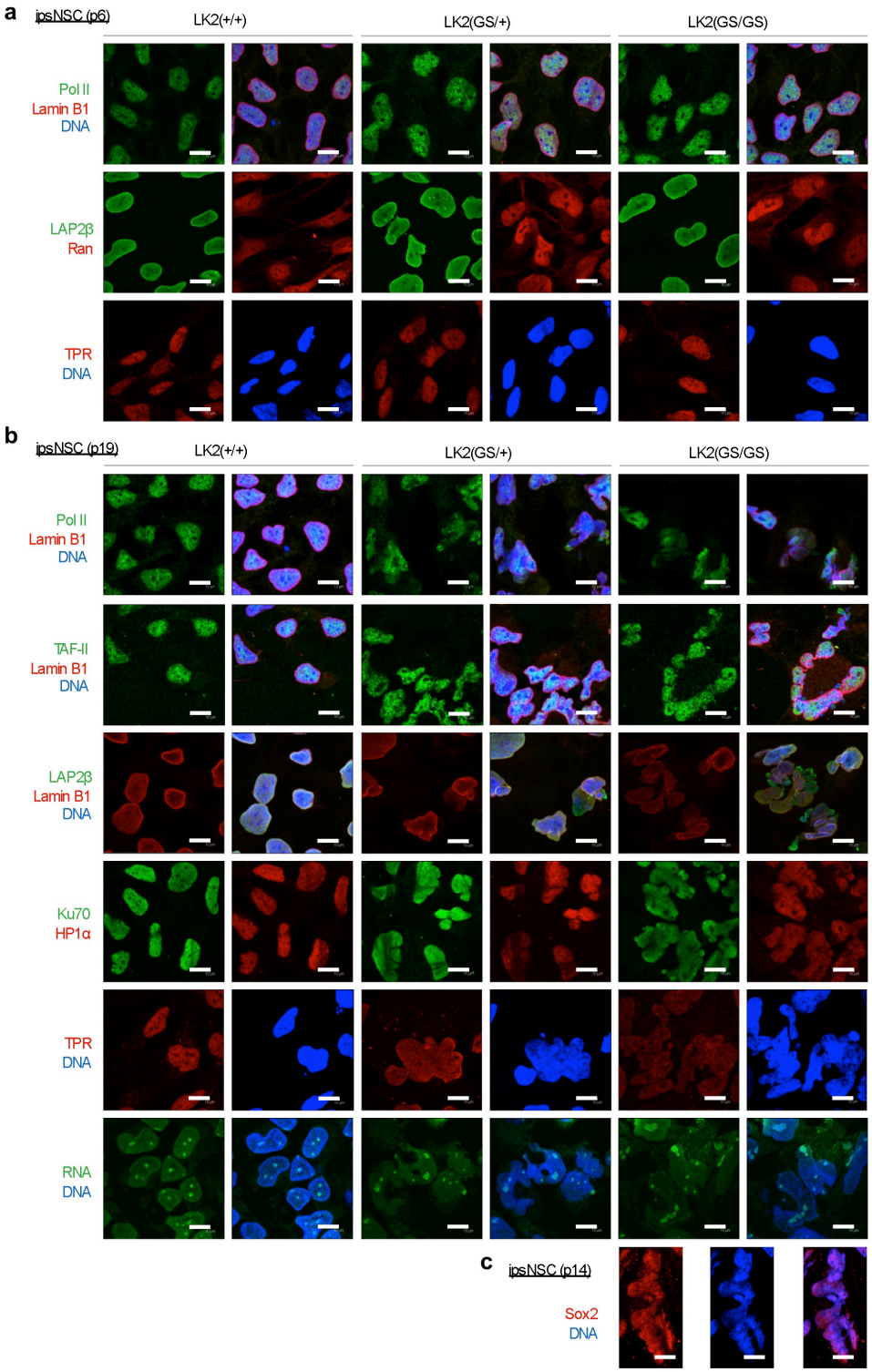

Supplementary Fig. 7. Localization of various nuclear components in wild-type and *LRRK2* G2019S NSCs. Immunofluorescence for the indicated proteins in ipsNSCs-LK2(+/+), ipsNSCs-LK2(GS/+) and ipsNSCs-LK2(GS/GS) at passage 6 (**a**), passage 19 (**b**), and passage 14 (**c**). Scale bars, 10 μm.

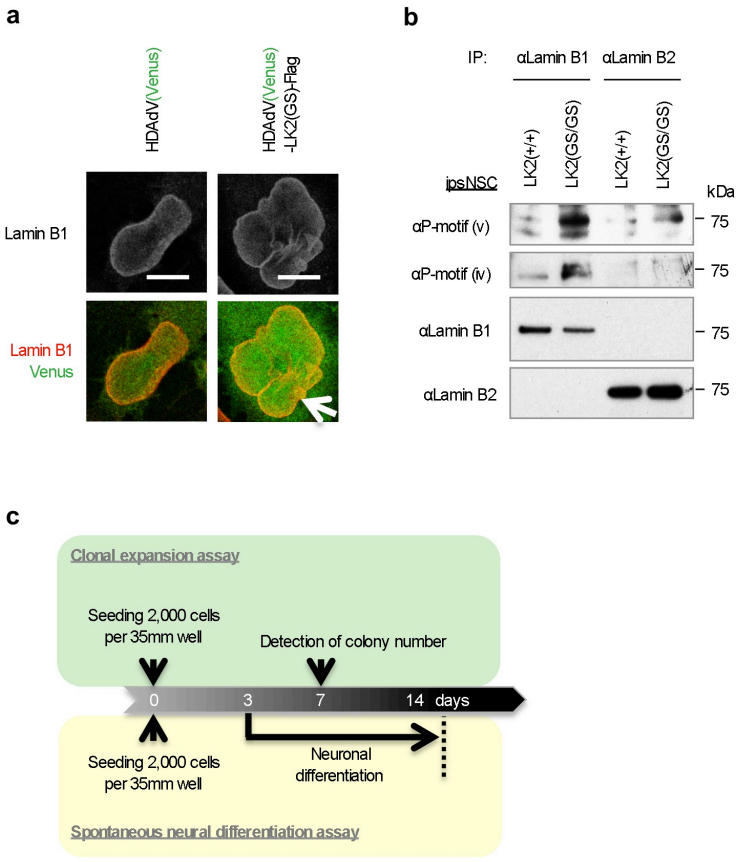

Supplementary Fig. 8. Overexpression of LRRK2(G2019S) cause abnormal nuclear morphology in NSCs. a, esNSCs were transduced with HDAdV(venus) and HDAdV(venus)-LK2(GS). 10 days later, cells were immunostained with anti-Lamin B1 antibody. Arrow indicates a deformed and enlarged nucleus caused by LRRK2(G2019S) overexpression. Scale bar, 10 μm. **b**, The same amount of cell lysate from passage 18 ipsNSCs-LK2(+/+) and ipsNSCs-LK2(GS/GS) were subjected to immunoprecipitation using either Lamin B1 or Lamin B2 antibody. The immunopurified Lamin B1 and Lamin B2 were then immunoblotted with the indicated anti-phosphorylated Ser/Thr motif antibodies described in **Supplementary Fig. 16a**. **c,** Schematic representation of clonal expansion and spontaneous neuronal differentiation strategy of NSCs.

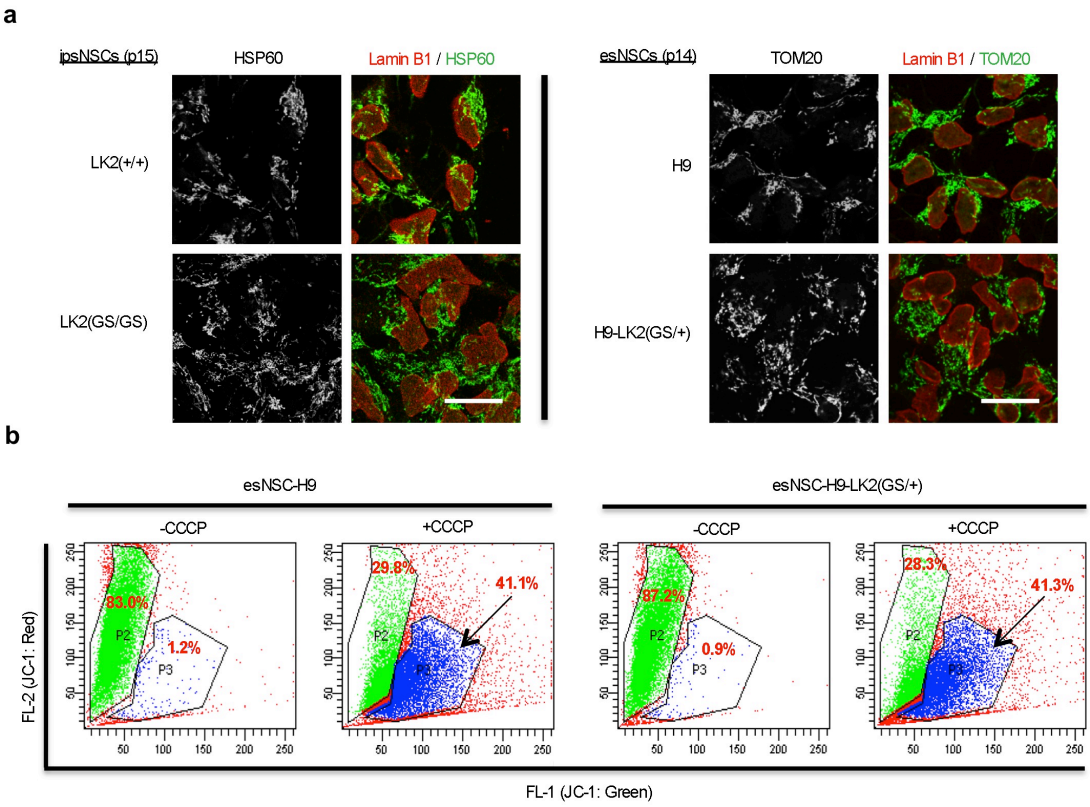

Supplementary Fig. 9. Mitochondrial parameters in wild-type and *LRRK2* G2019S NSCs. a, Immunofluorescence analysis of mitochondrial proteins in the indicated NSC lines. Scale bars, 20 μm. **b,** Flow cytometry analysis revealed no significant difference in basal and CCCP-stimulated mitochondrial membrane potentials($\Delta\Psi_{mito}$) between esNSCs-H9 and esNSCs-H9-LK2(GS/+) at passage 14. The percentages of cells with red (P2) and green (P3) JC-1 fluorescence represent high and low $\Delta\Psi_{mito}$, respectively.

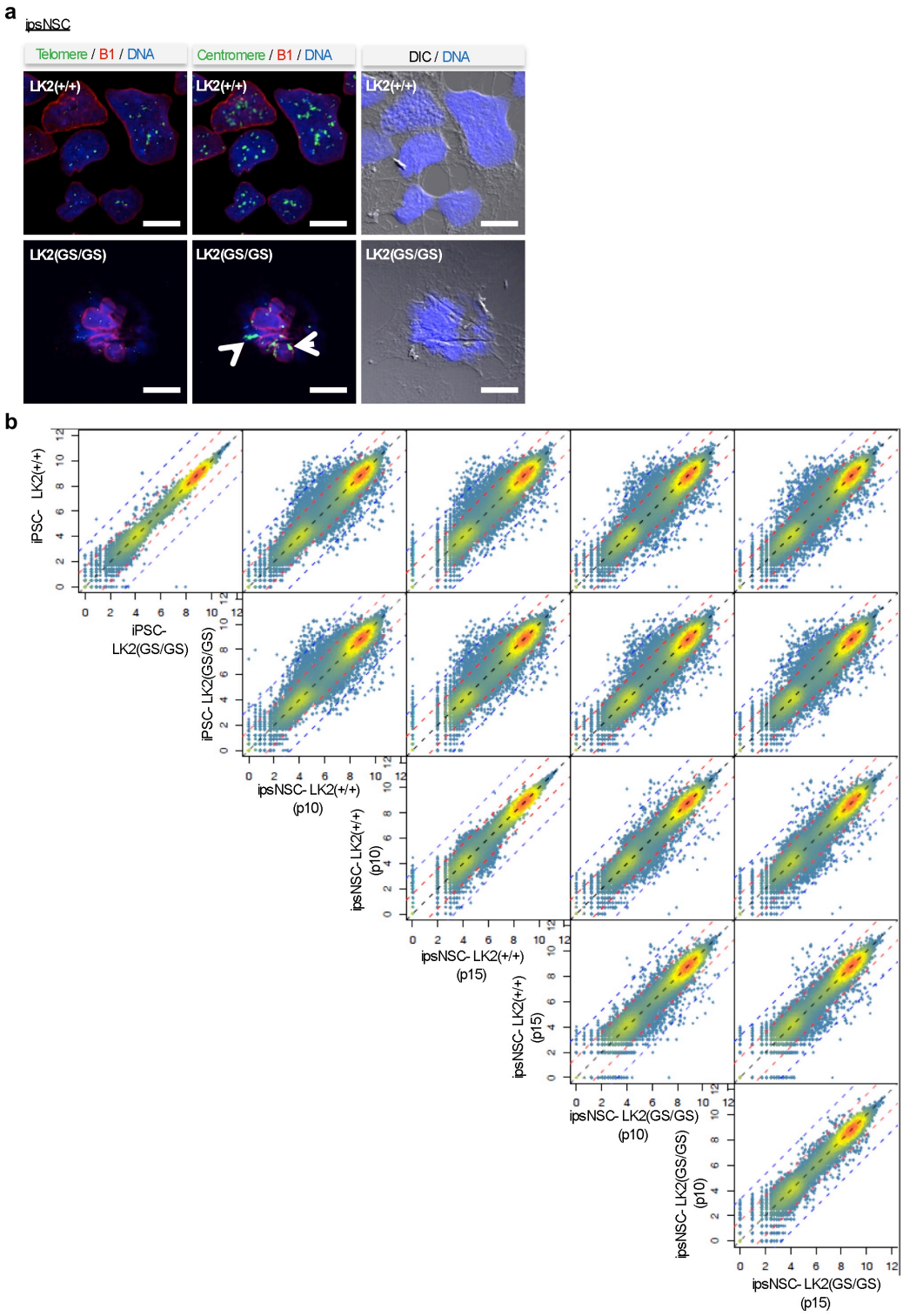

Supplementary Fig. 10. Chromatin organization in wild-type and *LRRK2* G2019S NSCs. a, 3D-fluorescence *in situ* hybridization (3D-FISH) analysis on nuclear localization of telomeric and centromeric heterochromatin in passage 15 ipsNSCs. Interphase nuclei were hybridized with a FAM-labeled telomere probe (green) and a Cy3-labeled centromere probe (pseudocolored green). Immunostaining for Lamin B1 (B1) was performed after FISH (visualized by Dylight 649-

conjugated secondary antibody, pseudocolored red). DNA was stained with DAPI. Cell morphology was visualized by differential interference contrast (DIC) microscopy. Arrows show examples of centromere clustering in ipsNSCs-LK2(GS/GS). Scale bars, 10 μm. **b,** Promoter-associated H3K4me3 levels show high genome-wide similarity between iPSCs and differences between ipsNSCs. Scatter plots show pair-wise comparisons of quantile normalized log2-read counts within +/-2.5 kb of the Transcription Start Site (TSS) or RefSeq genes. Data points are colored based on density ranging from blue (low density) through yellow to red (high density). Red and blue dashed lines mark a 3- and 5-fold difference in tag count, respectively.

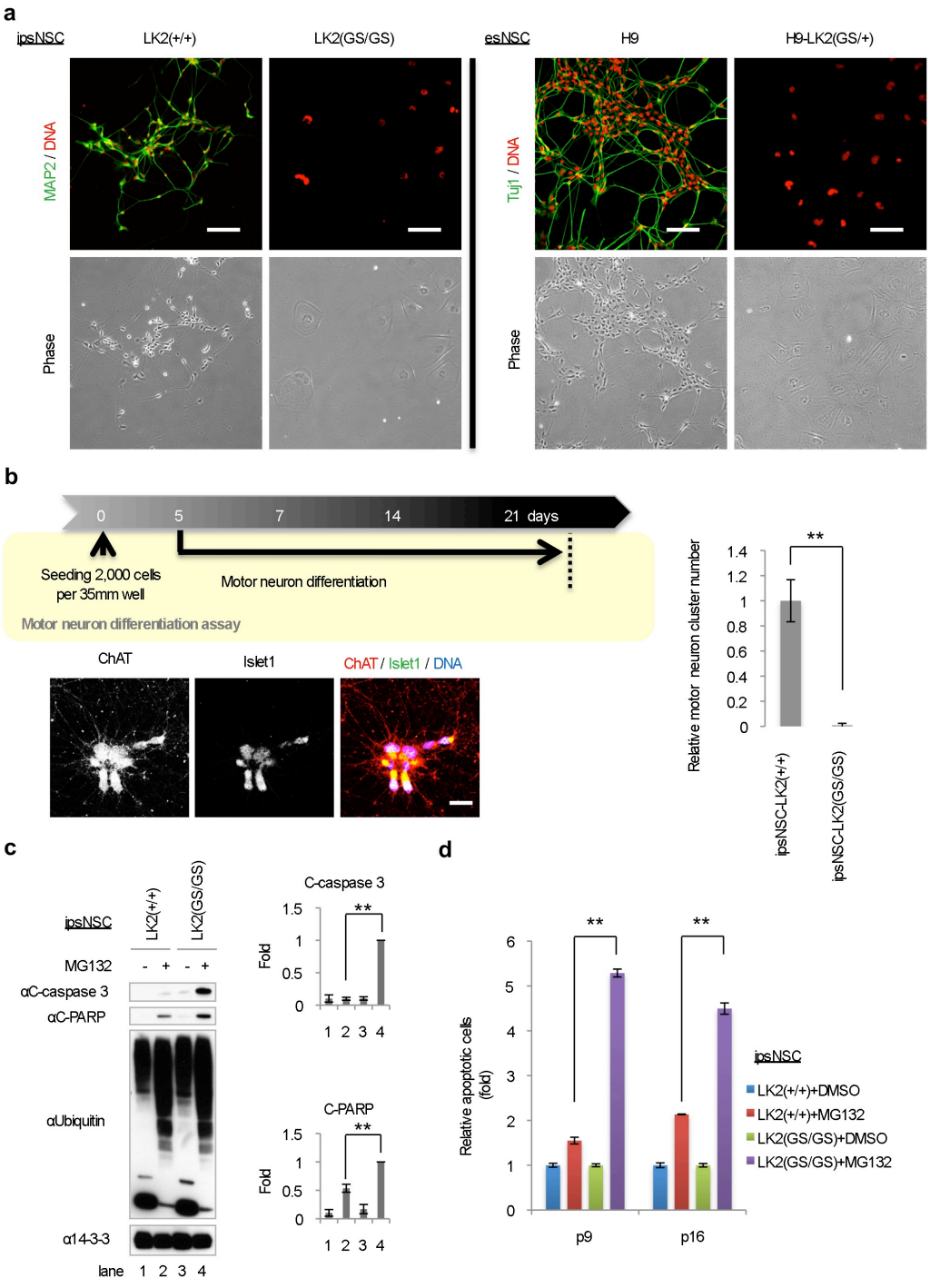

Supplementary Fig. 11. *LRRK2* G2019S mutant NSCs show abnormal phenotypes in single cell-based neuronal differentiation and proteasomal stress assays. a, Immunofluorescence analysis of the neuronal marker MAP2 (left panels) and Tuj1 (right panels) in representative spontaneous neuronal differentiation experiments. Under the same culture conditions, ipsNSCs-LK2(+/+) at passage 17 (left) and esNSCs-H9 at passage 14 (right) efficiently differentiated towards MAP2- or Tuj1-positive neurons, respectively, whereas ipsNSCs-LK2(GS/GS) at passage 17 (left) and esNSCs-H9-LK2(GS/+) at passage 14 (right) gave rise to MAP2- or Tuj1-negative cell derivatives, respectively, with non-neuronal morphology. Also see zoomed versions

in **Fig. 2c and Supplementary Fig. 14c**. Scale bars, 80 μm. **b,** Schematic representation of single cell-based motor neuron differentiation assay (upper left). Representative immunofluorescence images (lower left) for neuronal clusters expressing motor neuron markers ChAT and Islet1. Scale bar, 20μm. Quantification analysis of motor neuron cluster numbers derived from ipsNSCs-LK2(+/+) and ipsNSCs-LK2(GS/GS) at passage 17 (right plot). Data are shown as mean±s.d. n=3. **p<0.01. **c,** Representative immunoblot data (left panel) and quantification analysis (right panel) of cleaved caspase 3 (C-caspase 3), cleaved PARP (C-PARP), and ubiquitinated conjugates (Ubiquitin) in ipsNSCs-LK2(+/+) and ipsNSCs-LK2(GS/GS) at passage 15 untreated (-) or treated (+) with 10 μM MG132 for 20 h. 14-3-3 was used as loading control. Data are shown as mean±s.d. n=3. **p<0.01. **d,** ipsNSCs-LK2(+/+) and ipsNSCs-LK2(GS/GS) at passage 9 and 16 were treated with MG132 for 20 h and apoptotic cells were determined by Annexin V/PI flow cytometry analysis. Values of DMSO-treated groups were normalized to 1. Data are shown as mean±s.d. n=3. **p<0.01.

a

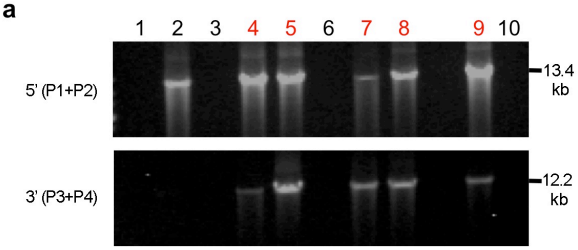

b

# of infected cells	# of G418^R GANC^R [a]	# of gene targeted clones [b]	gene targeting (%) [b/a x100]	# of gene correction clones [c]	gene correction (%) [c/a x100]
2x10^6	10	5	50	1	10

c

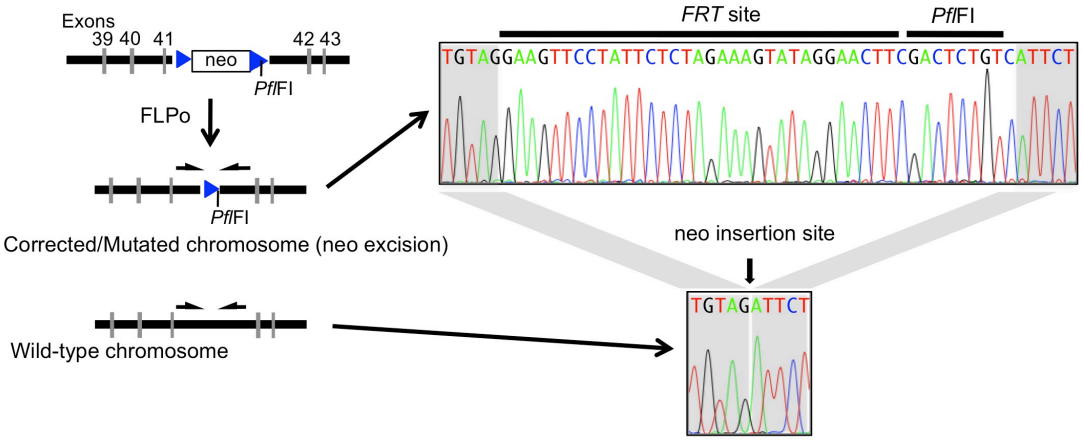

Supplementary Fig. 12. Gene correction in LK2(GS/+) iPSC lines by *LRRK2*-c-HDAdV. a, PCR analysis of *LRRK2* G2019S heterozygous mutant iPSCs (LK2(GS/+)) targeted with *LRRK2*-c-HDAdV using 5' primer pairs (P1+P2; 13.4 kb) and 3' primer pairs (P3+P4; 12.2 kb) shown in **Fig. 3a**. Red numbers indicate the number of gene-targeted clones which were positive for both 5' and 3' gene targeting. **b,** Gene-targeting and gene-correction efficiencies at the *LRRK2* genomic locus. **c.** Sequencing results showing that the neomycin-resistant cassette (neo) was successfully removed from intron 41 of *LRRK2* in the gene-corrected iPSCs by FLPo recombinase. Schematic demonstration of a 43 bp sequence (*FRT* and *Pfl*FI) left in intron 41 of the *LRRK2* locus after neo removal.

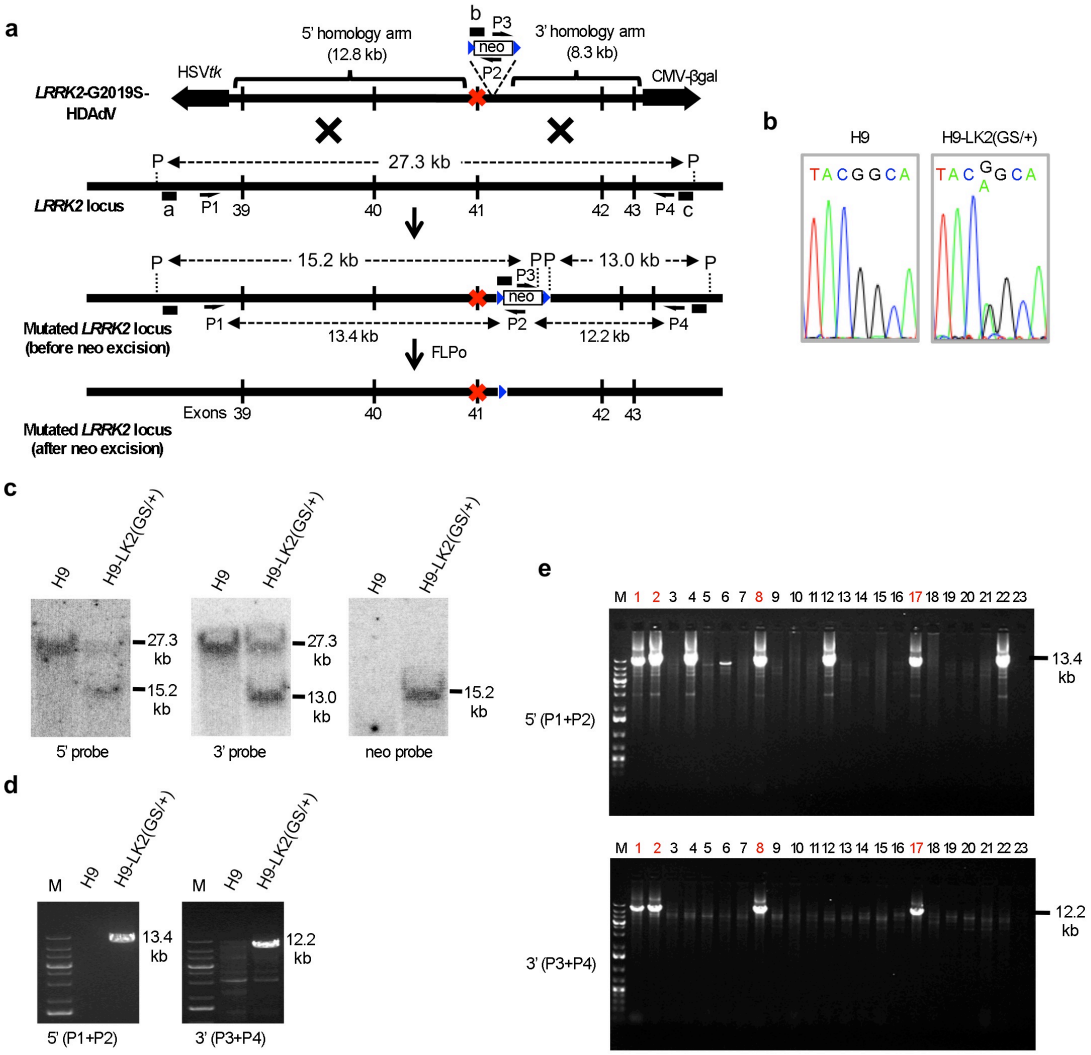

f

# of infected cells	# of GANC^R	G418^R [a]	# of gene targeted clones [b]	gene targeting (%) [b/a x100]	# of mutation knock-in clones [c]	mutation knock-in (%) [c/a x100]
1.25x10^6	23		4	17	4	17

Supplementary Fig. 13. *LRRK2*(G2019S) mutation knock-in in H9 ESCs by *LRRK2*-G2019S-HDAdV. a, Schematic representation of HDAdV-based knock-in of the G2019S mutation into the *LRRK2* gene. Half arrows indicate the primer sites for PCR (P1, P2, P3 and P4). The probes for Southern analysis are shown as black bars (a, 5' probe; b, neo probe; c, 3' probe). Red X indicates the mutation site in exon 41; blue triangles indicate FLPo recognition target (*FRT*) sites. P indicates *Pfl*FI sites. **b,** Sequencing results of the G2019S mutation site in exon 41 of the *LRRK2* gene in H9 hESCs before (left; H9) and after (right; H9-LK2(GS/+)) knock-in. **c,** Southern blot analysis of H9 hESCs and their mutant counterparts bearing neo cassette (H9-LK2(GS/+)) using the indicated probes. **d,** Representative PCR analysis of H9 hESCs and their mutant derivative H9-LK2(GS/+) using the indicated primer pairs. M indicates DNA ladder. **e**, PCR analysis of H9 ESCs targeted with *LRRK2*-G2019S-HDAdV using 5' primer pairs (P1+P2; 13.4 kb) and 3' primer pairs (P3+P4; 12.2 kb) shown in **a**. Red numbers indicate gene-targeted clones which were positive for both 5' and 3' gene targeting. **f,** Gene-targeting and mutation knock-in efficiencies at the *LRRK2* genomic locus.

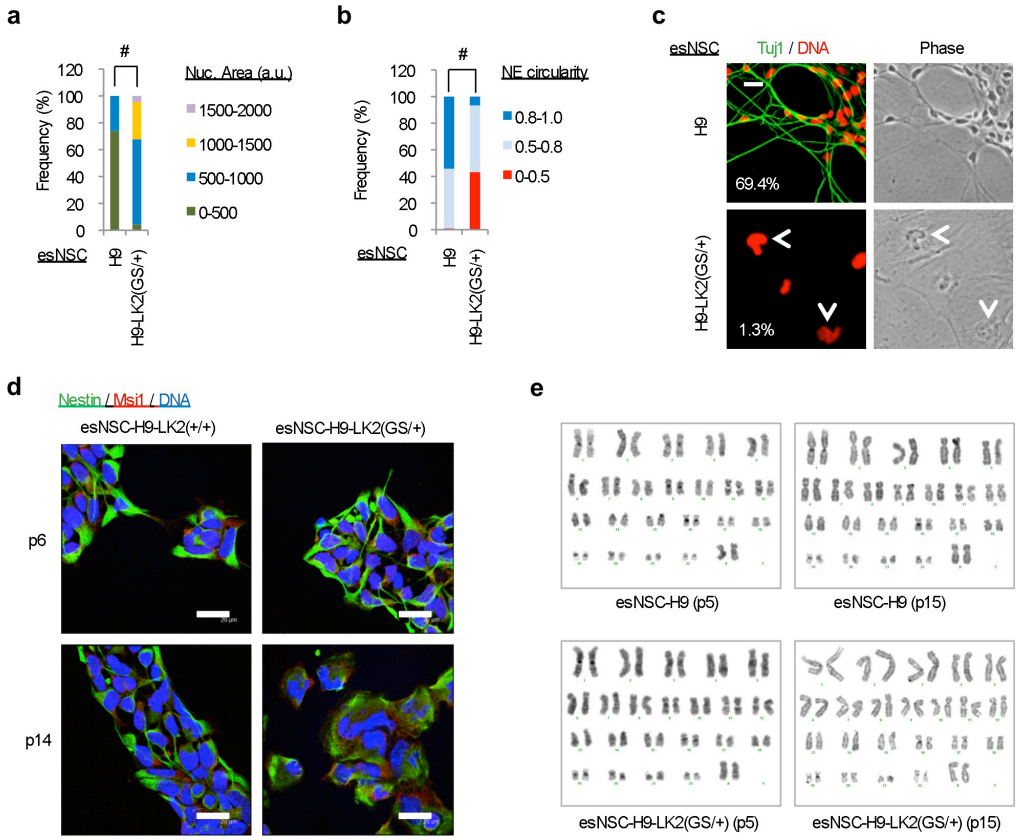

Supplementary Fig.14. Isogenic esNSCs with *LRRK2*(G2019S) mutation recapitulate the phenotypic defects observed in ipsNSCs-*LRRK2*(G2019S). a-b, Quantification of nuclear area (**a**) and nuclear envelope (NE) circularity (**b**) in esNSCs-H9 and esNSCs-H9-LK2(GS/+) at passage 14. a.u., arbitrary units. $^{\#}p<10^{-15}$. **c,** Immunofluorescence analysis for the neuronal marker Tuj1 in neurons spontaneously differentiated from esNSCs-H9 or esNSCs-H9-LK2(GS/+) at passage 14. Arrows indicate deformed nuclei. Percentages of neuronal differentiation efficiency, indicated by the ratio of Tuj1 positive cells to total cell nuclei, are shown in the corners. Also see **Supplementary Fig. 11a (right panels)** for wide field images. Scale bar, 20 μm. **d**, Immunostaining of NSC markers in esNSCs-H9 and esNSCs-H9-LK2(GS/+) at passage 6 (p6) and 14 (p14). DNA was stained with DAPI. Scale bars, 20 μm. **e,** Wild type esNSCs-H9 and mutation knock-in esNSCs-H9-LK2(GS/+) exhibited normal karyotypes at both early (p5) and late (p15) passages.

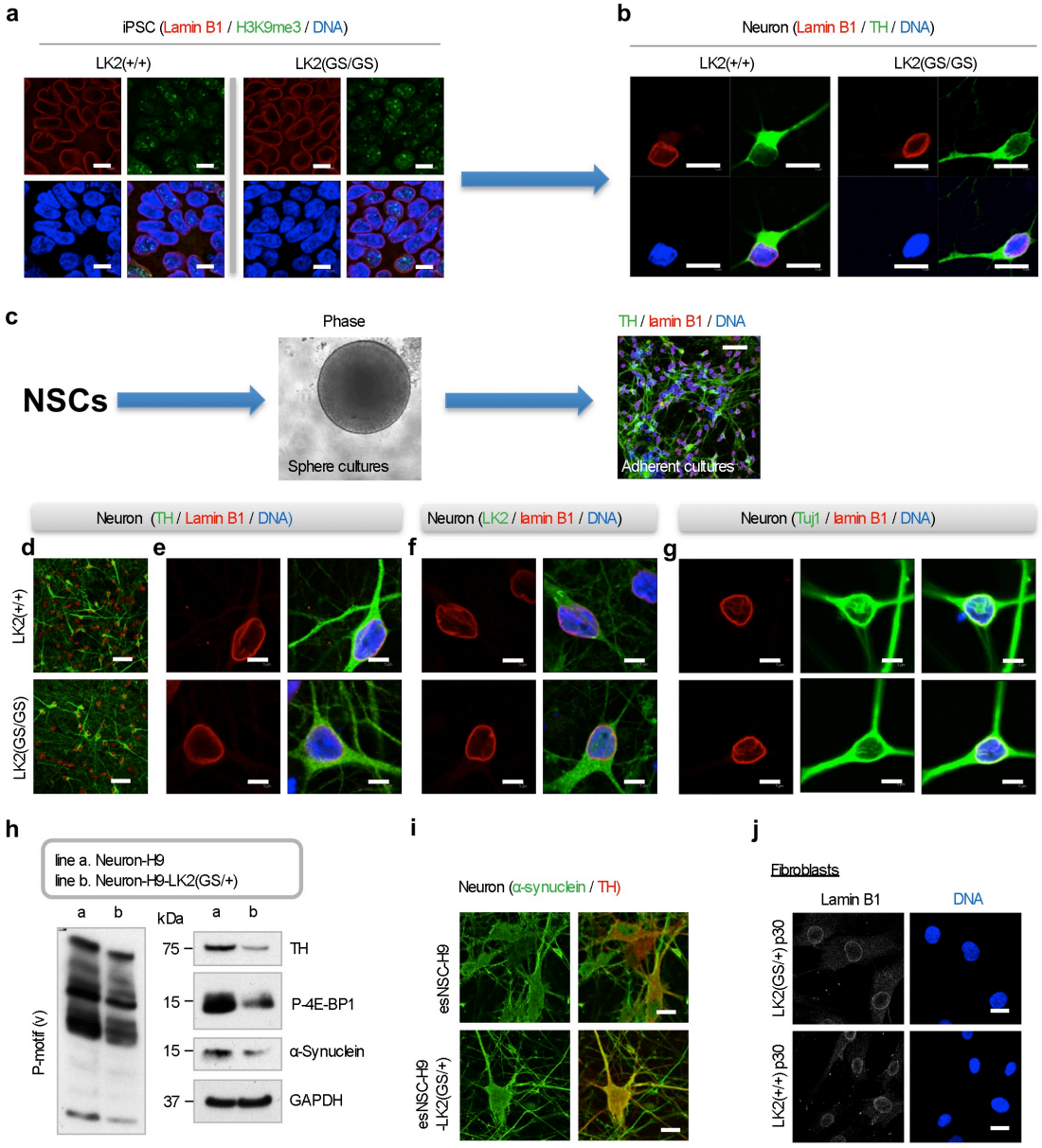

Supplementary Fig. 15. *LRRK2* G2019S-associated phenotypic defects are specific to NSCs and are not present in iPSCs, neurons or fibroblasts. a, Immunofluorescence analysis of Lamin B1 and H3K9me3 in the indicated iPSC lines (passage 40). DNA was counterstained with Hoechst. Scale bars, 10 μm. **b,** Immunofluorescence analysis of Lamin B1 and TH in the indicated iPSC-derived dopaminergic neurons (60 days in culture). DNA was counterstained with Hoechst. Scale bars, 10 μm. For (**a**) and (**b**), LK2(GS/GS)-iPSCs and their dopaminergic neuron derivatives show no discernible alteration in nuclear architecture. **c**, Schematic demonstration on derivation of dopaminergic neurons from passage 6 NSCs through a sphere-based technique. Scale bars, 40 μm. **d-g**, Dopaminergic neurons (**d-f**) and pan-neurons (**g**) derived from passage 6 ipsNSCs-LK2(+/+) and ipsNSCs-LK2(GS/+) show no discernible difference in nuclear envelope. Scale bars, 40 μm (**d**), and 5 μm (**e-g**). **h**, Immunoblot analysis of dopaminergic neurons (60 days in culture) derived from passage 6 esNSCs-H9 (line a, Neuron-H9) and esNSCs-H9-LK2(GS/+) (line b, Neuron-H9-LK2(GS/+)) with the indicated antibodies. The immunoblotting data did not show upregulation of target protein phosphorylation or α-synuclein in *LRRK2*(G2019S)

mutant dopaminergic neurons. **i**, Immunostaining of indicated proteins in dopaminergic neurons derived from passage 6 esNSCs-H9 and esNSCs-H9-LK2(GS/+). Scale bar, 10 μm. **j,** Immunofluorescence analysis of Lamin B1 in healthy donor (LK2(+/+)) derived- and *LRRK2* G2019S patient (LK2(GS/+)) derived-fibroblasts at passage 30. Scale bar, 20 μm.

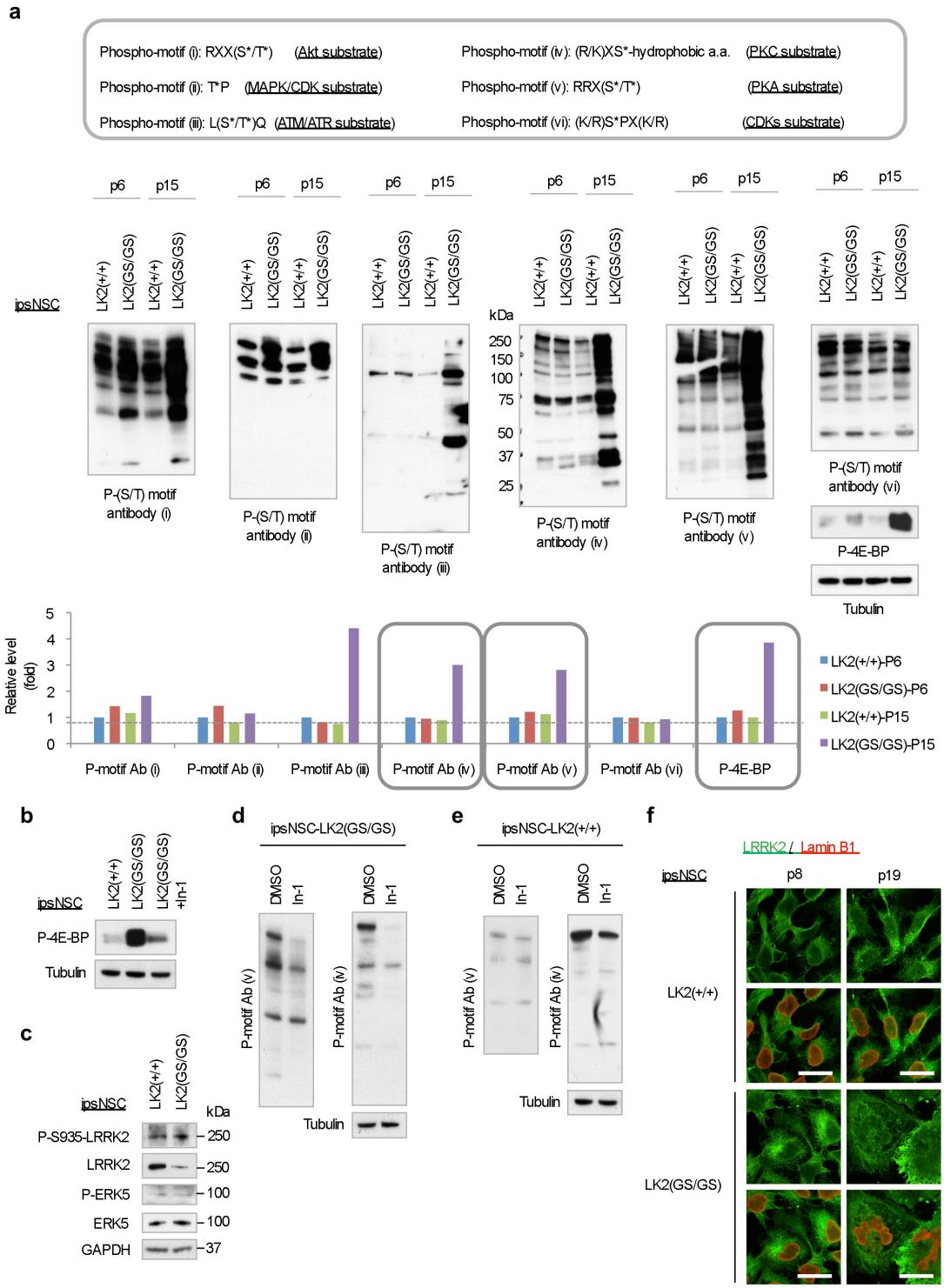

Supplementary Fig. 16. *LRRK2*(G2019S) mutation promotes activation of phosphorylated Ser/Thr substrate proteins in ipsNSCs. a, Upper box: Phosphorylated Ser/Thr motif specific antibodies used in this study. Blots**:** A total of 40,000 NSCs at passage 6 or 15 were directly lysed with SDS sample buffer and subjected to immunoblotting analysis, and various protein species were probed with indicated antibodies to assess their phosphorylation status. Tubulin was used as a loading control. Quantitative analyses of above blots are shown in the lower panel. **b**, 20 μg

of protein lysates from passage 15 ipsNSCs-LK2(+/+), ipsNSCs-LK2(GS/GS) and ipsNSCs-LK2(GS/GS) treated with 3 μM In-1 for 5 d were subjected to immunoblotting analysis with anti-phosphorylated 4E-BP and anti-4E-BP antibodies. Tubulin was used as a loading control. Blots are representative of three independent experiments. **c**, 20 μg of protein lysates from passage 15 ipsNSCs-LK2(+/+) and ipsNSCs-LK2(GS/GS) were subjected to immunoblotting analysis with anti-phosphorylated S935-LRRK2, anti-LRRK2, anti-phosphorylated ERK5 and anti-ERK5 antibodies. GAPDH was used as a loading control. Blots are representative of three independent experiments. **d-e,** Passage 15 ipsNSCs-LK2(GS/GS) (**d**) and ipsNSCs-LK2(+/+) (**e**) were treated with 3 μM In-1 for 3 days, and then 20 μg of cell lysates were probed with the indicated phosphorylated Ser/Thr motif antibodies. Consistent with recent report showing that wild-type LRRK2 is more resistant to LRRK2-In-1-mediated repression relative to its G2019S mutant (Deng et al, 2011), treatment of late passage ipsNSCs-LK2(+/+) showed marginal effects on protein phosphorylation profiles. Blots are representative of three independent experiments. **f,** Immunostaining of LRRK2 and Lamin B1 in ipsNSCs-LK2(+/+) and ipsNSCs-LK2(GS/GS) at the indicated passages. Scale bar, 20 μm.

a

	DMSO	LRRK2-In-1	Sunitinib	H1152	LY294002	PD98095	H89
Known target kinase(s)		LRRK2	(1) Receptor tyrosine kinases (main target) (2) LRRK2	(1)ROCK (main target) (2)LRRK2	PI3K	MAPK	PKA
Concentration	0.1%	3 μM	10 μM	30 μM	10 μM	10 μM	10 μM
References		Deng et al. 2011	Dzamko et al. 2010				
Treatment time (d)	5	5	3	5	5	5	5
Growth as tight colonies	N	Y	N	N	N	N	N
Rescue of nuclear morphology	N	Y	N	N	Y	N	N
Other phenotypes			Severe cell death after 3-d treatment	Dramatic change in cytoskeleton			

b

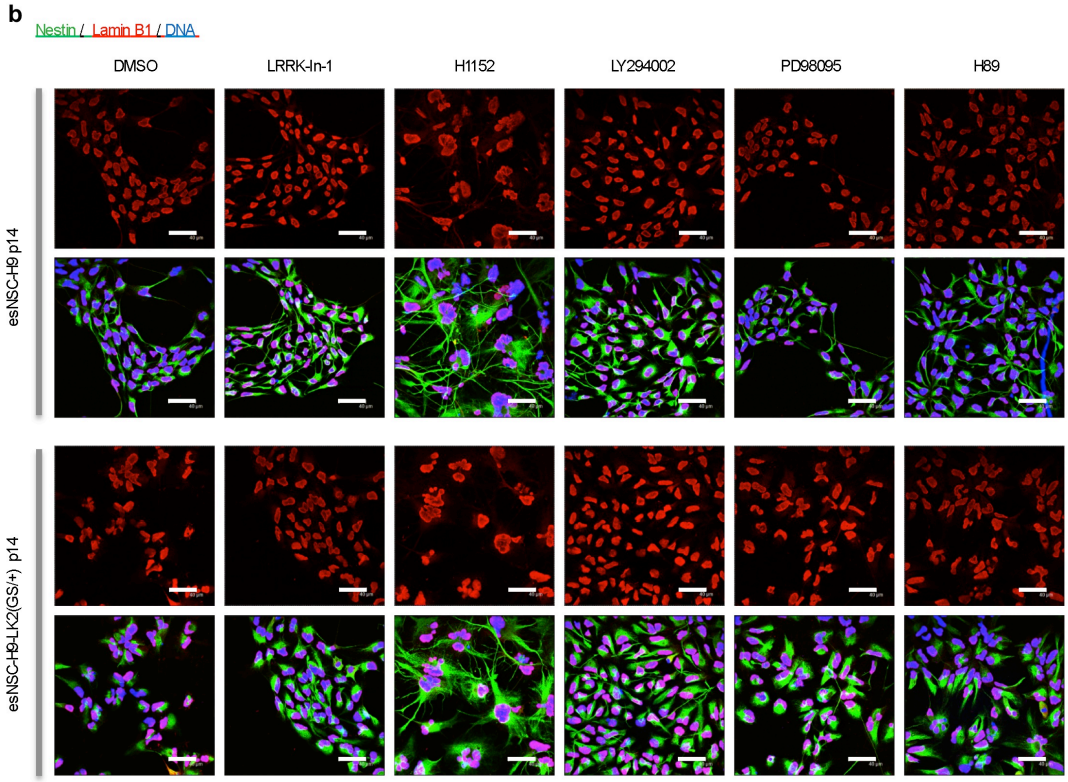

Supplementary Fig. 17. LRRK2-specific inhibitor (In-1) rescues the morphological defects in *LRRK2* G2019S NSCs. a-b, Passage 14 esNSCs-H9 and esNSCs-H9-LK2(GS/+) were treated with various kinase inhibitors (**a**), and then immunostained for Nestin (Green), Lamin B1 (Red), and nuclei (blue) (**b**). Note: Whereas receptor tyrosine kinases inhibitor Sunitinib at 10 μM and ROCK inhibitor H1152 at 30 μM have been shown to inhibit LRRK2 kinase activity in a recent report, we observed that treatment of esNSCs with 10 μM Sunitinib for 3 days caused severe cell death, and treatment of esNSCs with 30 μM H1152 triggered dramatic changes in the cytoskeleton. These observations could be explained by the predominant repressive effects of these two chemicals on receptor tyrosine kinases and ROCK, respectively. Scale bars, 40 μm. Y, show the indicated phenotype. N, do not show the indicated phenotype.

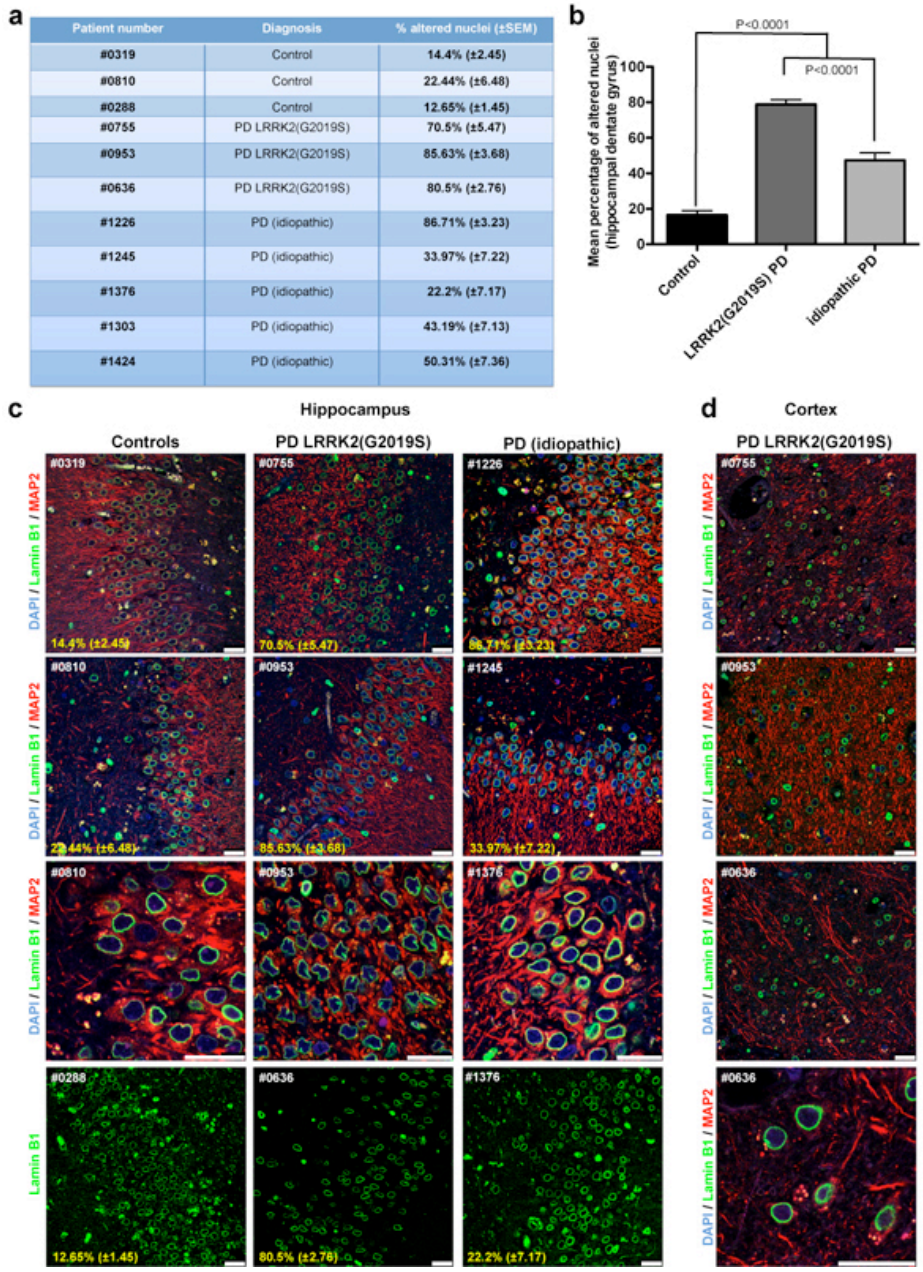

Patient number	Diagnosis	% altered nuclei (±SEM)
#0319	Control	14.4% (±2.45)
#0810	Control	22.44% (±6.48)
#0288	Control	12.65% (±1.45)
#0755	PD LRRK2(G2019S)	70.5% (±5.47)
#0953	PD LRRK2(G2019S)	85.63% (±3.68)
#0636	PD LRRK2(G2019S)	80.5% (±2.76)
#1226	PD (idiopathic)	86.71% (±3.23)
#1245	PD (idiopathic)	33.97% (±7.22)
#1376	PD (idiopathic)	22.2% (±7.17)
#1303	PD (idiopathic)	43.19% (±7.13)
#1424	PD (idiopathic)	50.31% (±7.36)

Supplementary Fig. 18. *LRRK2*(G2019S) human PD brain samples display abnormal nuclear morphologies. a, summary table of all patient samples analyzed and the respective percentage of aberrant nuclei in the hippocampal dentate gyrus. **b,** quantification of aberrant nuclei present in the dentate gyrus observed in the different patient samples. Note that LRRK2(G2019S) (n=3) displays significantly higher numbers of aberrant nuclei as compared to both, control (n=3) as well as idiopathic samples (n=5). Data are shown as mean±s.e.m. **c,d** representative pictures of analyzed human brain samples. Lamin B1 staining demonstrates prominent disruption of the nuclear envelope in *LRRK2*(G2019S)-bearing Parkinson patients in neurogenic areas (**c**) as compared to idiopathic and control samples. Brain cortex, a non-neurogenic area, serves as internal negative control (**d**). Percentages ± s.e.m. indicate the number of aberrant nuclei observed. Scale bars, 25 μm.

Supplementary References

1. Kanao, T. et al. Activation of FoxO by LRRK2 induces expression of proapoptotic proteins and alters survival of postmitotic dopaminergic neuron in Drosophila. *Hum Mol Genet* **19**, 3747-3758 (2010).
2. Nagai, T. et al. A variant of yellow fluorescent protein with fast and efficient maturation for cell-biological applications. *Nat Biotechnol* **20**, 87-90 (2002).
3. Liu, G.H. et al. Recapitulation of premature ageing with iPSCs from Hutchinson-Gilford progeria syndrome. *Nature* **472**, 221-225 (2011).
4. Li, W. et al. Rapid induction and long-term self-renewal of primitive neural precursors from human embryonic stem cells by small molecule inhibitors. *Proc Natl Acad Sci U S A* **108**, 8299-8304 (2011).
5. Morizane, A., Doi, D., Kikuchi, T., Nishimura, K. & Takahashi, J. Small-molecule inhibitors of bone morphogenic protein and activin/nodal signals promote highly efficient neural induction from human pluripotent stem cells. *J Neurosci Res* **89**, 117-126 (2011).
6. Liu, G.H. et al. Regulation of myoblast differentiation by the nuclear envelope protein NET39. *Mol Cell Biol* **29**, 5800-5812 (2009).
7. Washburn, M.P., Wolters, D. & Yates, J.R., 3rd Large-scale analysis of the yeast proteome by multidimensional protein identification technology. *Nat Biotechnol* **19**, 242-247 (2001).
8. Liu, G.H. et al. Recapitulation of premature ageing with iPSCs from Hutchinson-Gilford progeria syndrome. *Nature* (2011).
9. Hawkins, R.D. et al. Distinct epigenomic landscapes of pluripotent and lineage-committed human cells. *Cell Stem Cell* **6**, 479-491 (2010).
10. Langmead, B., Trapnell, C., Pop, M. & Salzberg, S.L. Ultrafast and memory-efficient alignment of short DNA sequences to the human genome. *Genome Biol* **10**, R25 (2009).
11. Li, H. et al. The Sequence Alignment/Map format and SAMtools. *Bioinformatics* **25**, 2078-2079 (2009).
12. Huang da, W., Sherman, B.T. & Lempicki, R.A. Bioinformatics enrichment tools: paths toward the comprehensive functional analysis of large gene lists. *Nucleic Acids Res* **37**, 1-13 (2009).
13. Datsenko, K.A. & Wanner, B.L. One-step inactivation of chromosomal genes in Escherichia coli K-12 using PCR products. *Proc Natl Acad Sci U S A* **97**, 6640-6645 (2000).
14. Shayakhmetov, D.M. et al. Genome size and structure determine efficiency of postinternalization steps and gene transfer of capsid-modified adenovirus vectors in a cell-type-specific manner. *J Virol* **78**, 10009-10022 (2004).
15. Palmer, D.J. & Ng, P. Physical and infectious titers of helper-dependent adenoviral vectors: a method of direct comparison to the adenovirus reference material. *Mol Ther* **10**, 792-798 (2004).
16. Suzuki, K. et al. Highly efficient transient gene expression and gene targeting in primate embryonic stem cells with helper-dependent adenoviral vectors. *Proc Natl Acad Sci U S A* **105**, 13781-13786 (2008).
17. Raymond, C.S. & Soriano, P. High-efficiency FLP and PhiC31 site-specific recombination in mammalian cells. *PLoS One* **2**, e162 (2007).